Chemistry, transport and dry deposition of trace gases in the boundary layer over the tropical Atlantic Ocean and the Guyanas during the GABRIEL field campaign

A. Stickler, H. Fischer, H. Bozem, C. Gurk, C. Schiller, M. Martinez-Harder, D. Kubistin, H. Harder, J. Williams, G. Eerdekens, et al.

HAL Id: hal-00302703
https://hal.science/hal-00302703

**Atmospheric
Chemistry
and Physics
Discussions**

Chemistry, transport and dry deposition of trace gases in the boundary layer over the tropical Atlantic Ocean and the Guyanas during the GABRIEL field campaign

A. Stickler[1,**], H. Fischer[1], H. Bozem[1], C. Gurk[1], C. Schiller[2],
M. Martinez-Harder[1], D. Kubistin[1], H. Harder[1], J. Williams[1], G. Eerdekens[1],
N. Yassaa[1], L. Ganzeveld[1,*], R. Sander[1], and J. Lelieveld[1]

[1]Department of Atmospheric Chemistry, Max Planck Institute for Chemistry, Mainz, Germany
[2]Department of Chemistry, York University, Toronto, Canada
[*]now at: Department of Earth System Science, University Wageningen, The Netherlands
[**]now at: Institute for Atmospheric and Climate Science, ETH Zürich, Switzerland

Title Page	
Abstract	Introduction
Conclusions	References
Tables	Figures
◀◀	▶▶
◀	▶
Back	Close
Full Screen / Esc	
Printer-friendly Version	
Interactive Discussion	

EGU

Abstract

We present a comparison of different Lagrangian and steady state box model runs with measurement data obtained during the GABRIEL campaign over the tropical Atlantic Ocean and the rainforest in the Guyanas, October 2005. Lagrangian modelling

of boundary layer (BL) CO constrained by measurements of reactive trace gases and radiation is used to derive a horizontal gradient (≈ 5.6 pmol/mol km^{-1}) of this compound from the ocean to the rainforest (east to west). This is significantly smaller than that derived from the measurements (16–48 pmol/mol km^{-1}), indicating that photochemical production from organic precursors alone cannot explain the observed strong gradient.

It appears that HCHO is overestimated by the Lagrangian and "steady state" models, which include dry deposition but not exchange with the free troposphere (FT). The relatively short lifetime of HCHO (50–100 min) implies substantial BL-FT exchange. The mixing-in of FT air affected by African and South American biomass burning at an estimated rate of 0.12 h^{-1} increases the CO and lowers the HCHO mixing ratios,

leading to a better agreement with measurements. A 24 h mean deposition velocity of 1.35 cm/s for H_2O_2 over the ocean as well as over the rainforest is deduced assuming BL-FT exchange adequate to the results for CO. The measured increase of the organic peroxides from the ocean to the rainforest (≈ 0.66 nmol/mol d^{-1}) is significantly overestimated by the Lagrangian model, even when using high values for the

deposition velocity and the entrainment rate. Our results point at either heterogeneous loss of organic peroxides and/or their radical precursors or a missing reaction path of peroxy radicals not forming peroxides in isoprene chemistry. We calculate a mean integrated daytime net ozone production (NOP) in the BL of (0.2±5.9)nmol/mol (ocean) and (2.4±2.1) nmol/mol (rainforest). The NOP strongly correlates with NO and shows

a positive tendency in the boundary layer over the rainforest.

1 Introduction

Despite the relatively small coverage of less than about 8% of the global land surface by tropical rainforests (areas classified as evergreen broadleef forests in Loveland et al., 2000), these regions are known to be a major global source of reactive trace
5 gases, primarily through vegetation emissions, partly because of the diverse and opulent flora and also because biogenic emissions are generally stimulated by high temperatures and/or irradiation intensity (see e.g. Kesselmeier and Staudt, 1999; Padhy and Varshney, 2005; Carvalho et al., 2005). These trace gases have a strong impact on the atmospheric oxidation capacity (e.g. Fehsenfeld et al. (1992)). The Amazon
10 basin including the Guyanas comprises the largest rainforest ecosystem worldwide. Although the region is perturbed by deforestation and burning, especially the Guyanas offer opportunities for atmospheric research in a relatively pristine environment. The region of the Guyanas (see Fig. 1) is characterised by low-level north-easterly and east-southeasterly trade winds, respectively, during both dry seasons from February to
15 March and from August to November. Therefore strong horizontal trace gas gradients can develop due to the build-up of oxidation products of the biogenic emissions that emerge from the forest. To assess the atmospheric fate of a trace gas, the ratios of its various chemical and physical lifetimes can be used, defined as the concentration divided by the respective loss rate (see e.g. Finlayson-Pitts and Pitts, 2000).
20   In this context, zero-dimensional or so-called box models as well as 1-D models have proven to be successful numerical tools to evaluate the relative importance of different chemical or physical processes influencing trace gas mixing ratios (e.g. Ganzeveld et al., 2006a,b; Stickler et al., 2006). However, when comparing box model results with measurement data it is important to ensure that some basic implicit assumptions are
25 fulfilled, namely that a) the air has to be well mixed and b) the amount of mixing-in of air with known properties from the surrounding domain as well as possible physical sinks of trace gases like deposition have to be known. The simplest case is one without exchange and deposition, which is assumed to be true e.g. in free tropospheric "steady

state" calculations of radical species and sometimes also for longer-lived species. In the planetary boundary layer (BL) on the other hand, dry deposition cannot be neglected for many trace gases (e.g. HNO_3, HCHO and peroxides) if there exists a thermally unstable stratification or wind shear leading to fast turbulent downward transport towards the surface at a timescale shorter than their chemical lifetime. Conversely, these turbulent motions are a necessary prerequisite for the required homogeneity inside the studied "box". In the case of relatively undisturbed conditions, the tropical BL can be expected to be best mixed from the late morning to the early evening. Its well-mixed state is characterised by a nearly constant potential temperature and wind speed profile (e.g. Holton, 1992). Under these circumstances, if only entrainment from the FT or deposition is unknown, it can in principle be estimated from a numerical simulation with the other parameters fixed to measured values. The GABRIEL campaign in October 2005 was planned as a follow-up project of the 1998 LBA-CLAIRE experiment, focussed on investigating the biosphere-atmosphere exchange of natural trace gases and quantifying chemical processes in the atmosphere over the tropical forest. The payload of the aircraft, a Learjet 35A of the Gesellschaft für Flugzieldarstellung (GFD, Hohn, Germany) based at Johann A. Pengel International Airport at Zanderij (see Fig. 1), was extended compared to LBA-CLAIRE, e.g. with additional in situ peroxide (H_2O_2 and organic peroxide), HCHO, and the first reported HO_x measurements over the tropical rainforest. Flights were conducted in a region from 3° N 59° W to 6° N 51° W over the tropical Atlantic Ocean, mainly northeast of the coastline of French Guyana, as well as over continental regions of Guyana, Suriname and French Guyana, which are mostly covered by tropical rainforest. The flight patterns were designed to allow for sampling both in the BL and in the FT. The flight paths generally included an ascent up to an altitude of about 6.5 to 8 km a.s.l. after take-off and a descent into the BL ($\approx$300–500 m a.s.l.) followed by alternating legs in the BL and the FT up to an altitude of about 3 to 3.5 km. The flight pattern was in most cases completed by another ascent to relatively higher levels above 5 to 6 km before landing. During flights 4 and 7 a third ascent was introduced in the middle of the flight. Flights 8 and 9 exhibited quite

Chemistry, transport and dry deposition of trace gases during GABRIEL

A. Stickler et al.

different altitude profiles. During flight 8 only one transit from the BL into the FT was performed in the middle of the flight, and a high ascent up to 11 km a.s.l. was used to study the upper tropospheric outflow of a rapidly developing convective cell. The profile of flight 9 was characterised by the aircraft staying essentially in the FT with a longer flight leg in the middle troposphere at about 5 km altitude and only one relatively short dive into the BL during the second half of the flight.

Sect. 2 shortly summarises the measurements carried out to obtain the data set used in this study. Section 3 describes the box model used to analyse the data and the boundary conditions for the Lagrangian and "steady state" mode as derived from the measurements and a 1-D Single Column Model (SCM). Section 4 presents results of different model runs, compares these with the trace gas measurements and interprets the data set. The role of chemistry, transport and dry deposition for CO, HCHO, H_2O_2 and organic peroxide is examined for typical "low NO_x" (approx. <20–25 pmol/mol, no direct influence by biomass burning) boundary layer conditions over the tropical Atlantic Ocean and the rainforest of the Guyanas during the long dry season.

2 Measurements

CO and HCHO were measured with the Tunable Diode Laser Absorption Spectrometer (TDLAS) TRISTAR (TRacer InSitu TDLAS for Atmospheric Research) which was modified to work with quantum cascade lasers instead of lead salt diode lasers. The inlet was connected to a 1/2" PTFE bypass and consisted of unheated 1/4" PTFE tubing. Ambient air was sampled with a cell exchange time of 6 s. The original data was stored each 4 s with 2 s measurement time for every data point. Calibrations were performed in-flight about every 10 min, and the standard used was compared to a secondary standard certified with respect to the NIWA scale (Brenninkmeijer et al., 2001). The estimated uncertainty of the CO data is 2.5% with a detection limit (DL) of 0.2 nmol/mol. HCHO data were additionally averaged over a range of ±60 s. Here the detection limit is 231 pmol/mol (1σ empirical standard deviation of the 2 min average of all background

measurements). The precision was estimated to be 17.6% at 5.4 nmol/mol (1σ empirical standard deviation of the 2 min average of all calibrations) or 25% at 1.0 nmol/mol, while the accuracy of the calibration standard, a permeation source, was calculated to be 10%. This results in a value of 20.2% at 5.4 nmol/mol or 26.9% at 1.0 nmol/mol for the total uncertainty.

Peroxides (H_2O_2 and total organic peroxides) were quantified based on the two-channel chemical derivatisation and fluorescence detection technique described originally in Lazrus et al. (1985) and Lazrus et al. (1986). While the instrument itself was kept unaltered compared to its status specified in Stickler et al. (2006) and Stickler (2006) for the UTOPIHAN aircraft measurement campaign, the setup of the inlet had to be changed. The constant pressure inlet used during UTOPIHAN could not be mounted onto the aircraft due to space limitations in the cabin since the instrumentation was extended (HO_x measurements). This implies that peroxide measurements could only be performed below a pressure altitude of 500 hPa corresponding to a geometrical altitude of about 5.5 km a.s.l.. The unheated, backward sampling inlet was constructed such that it switched to drawing cabin air over a bypass for zeroing of the instrument whenever the ambient pressure measured at the beginning of the inlet fell below a value of 500 hPa. When the pressure exceeded 800 hPa again (higher value due to technical reasons concerning the liquid flow inside the instrument), the cabin valve switched back to the regular measurement mode. The precision of the instrument for H_2O_2 was estimated to be 9.7% at a mixing ratio of 300 pmol/mol with a DL of 29 pmol/mol. Accuracy was calculated to be 14.8% at an H_2O_2 mixing ratio of 300 pmol/mol and an O_3 mixing ratio of 100 nmol/mol. The correction due to a known ozone interference of the instrument leads to a systematic error of $< +25$–30% for the H_2O_2 measurements throughout the troposphere. An upper limit estimate of the organic peroxide mixing ratio was derived assuming that the stripping efficiency for the mix of organic peroxides has a constant value of 80% and that the inlet efficiency, i.e. the fraction passing through the inlet without loss, has a value of 100%. An upper estimate for the total peroxide was calculated for flights 5 and 7 due to problems with the

organic peroxide channel assuming a stripping efficiency of 95% and an inlet efficiency of 85% (both derived using an estimated ratio H_2O_2/org. peroxide of 3.25). For the estimation of the error of the total peroxide mixing ratios, an additional relative error due to the stripping efficiency and the composition of the organic peroxide of ±20% is used (the stripping efficiency of all organic peroxides lies between that of CH_3OOH (60%) and that of H_2O_2 (100%)). This gives an accuracy of 24.9% at 0.3 nmol/mol. The precision is better than that of H_2O_2, because at first approximation the calculations use only one channel of the instrument and not the difference. Consequently, the DL is estimated to be smaller than that of H_2O_2.

OH and HO_2 were measured with the newly developed HORUS instrument[1], installed in one of two wingpods mounted on the aircraft. The system is based upon the Laser Induced Fluorescence (LIF) technique. The original 5 Hz data, alternating between signal and background measurement every 5 s, was averaged over 30 s. The DL of the system (2σ) was determined to be 0.02 pmol/mol for OH and 0.07 pmol/mol for HO_2 for 1 min averages with precisions (1σ, 1 min integration time) of 0.025–0.035 pmol/mol (OH) and 0.25–0.5 pmol/mol (HO_2), depending on the flight altitude (lower in the upper troposphere). The accuracy (2σ) for OH was estimated to be 40% in general except for two flights, for which the in-flight calibrations could not be evaluated due to missing water vapour measurements and a higher value of 56% was calculated. Water vapour data was available for a total of 42% of the HO_x data. When no water vapour data was available, the precision of the HO_x measurements includes an additional systematic error of up to 6.5% (2.6% on average) of the determined mixing ratios.

NO and O_3 mixing ratios were measured with ECOEX, a modified ECO-Physics SR790 HS instrument, using the chemiluminescence technique and adding NO as titration gas in the O_3 channel. The unheated 1/4" PTFE inlet was connected to a 1/2" bypass shared with the PTR-MS (see below). Sampled air had a residence time of

---

[1]A detailed discussion can be found in Martinez et al. (2007), Atmos. Chem. Phys. Discuss., in preparation, 2007.

Chemistry, transport and dry deposition of trace gases during GABRIEL

A. Stickler et al.

at most 1 s in the inlet. Data were taken as 1 s averages. The accuracy of the NO measurements was determined to be 12% with a DL of 5 pmol/mol (1σ). For O_3 the corresponding values are 2% and 2 nmol/mol. $J(NO_2)$ photolysis rates were measured using modified METCON filter radiometers. Precision and accuracy of these measure-
5 ments are 1% and 10% respectively.

Several volatile organic compounds were measured by means of Proton Transfer Reaction Mass Spectrometry (PTR-MS). Only 5 mass-to-charge ratios are implemented in this study: methanol (m/z 33), acetonitrile (m/z 42), acetone (m/z 59), isoprene (m/z 69), and the sum of methacrolein and methyl vinyl ketone (collectively measured
10 at m/z71, denoted MVK hereafter). Measurements by the PTR-MS are composite quantities where multiple signals, each with their own precision and accuracy, must be combined in order to obtain a final result. Here, the precision or the statistical uncertainty in the volume mixing ratio was calculated conservatively using the rule of error propagation. Measurement of each species was made once almost every 30 s with
15 dwell times of 0.5–2 s per mass. Using counting statistics for these times and propagation of error yields a median precision of 39% for methanol (with a median mixing ratio of 2.08 nmol/mol), 20% for acetonitrile (median of 0.166 nmol/mol), 17% for acetone (median of 0.7 nmol/mol), 7% for isoprene (median 2.05 nmol/mol) and 12% for MVK (median of 0.97 nmol/mol) for data sampled within the boundary layer between
20 9:00 and 16:00 (UT + 3 h). The accuracy excluding precision depends on the accuracy of each signal used in the calculation and their respective systematic errors. Reported values are estimated to be accurate to within 5-10% assuming no unaccounted systematic errors are present and using the accuracy of the calibration standard and measurements of the calibrated instrument response. If noise at each channel is taken
25 as the signal observed when sampling zero air (sampling with a catalytic converter in-line), the DLs for the unsmoothed data using a threshold signal-to-noise ratio of three were 0.269 nmol/mol (methanol), 0.068 nmol/mol (acetonitrile), 0.094 nmol/mol (acetone), 0.099 nmol/mol (isoprene) and 0.093 nmol/mol (MVK).

Water vapour and CO_2 were detected with the FABLE instrument, a commercially

available LI-COR infrared analyser adapted to aircraft measurements. The unheated, backward facing inlet consisted of 3/8" stainless steel. The DL of the instrument for H_2O is 200 μmol/mol with an overall uncertainty of 5%. For CO_2, the measurements take place in a range far above the DL and the uncertainty has been estimated as 0.3

5 μmol/mol. Ambient air was sampled with a cell exchange time of 3 s and the data was stored with a 1 s resolution.

Flight data (latitude, longitude, aircraft heading, wind speed, wind angle, drift angle, cabin temperature, static pressure, cabin pressure, aircraft generator DC voltage, altitude, static air temperature and true air speed) were acquired from the aircraft flight

10 management system and the Enviscope data acquisition system (Enviscope, Frankfurt (Germany)). Measured parameters, precisions and accuracies are listed in Table 1.

3   Box model

3.1   Model description

The box model is based on a version used previously to determine the influence of

15 summertime deep convection on the formaldehyde budget over Europe by Stickler et al. (2006) and Stickler (2006). It contains the MECCA v0.1p chemical mechanism (Sander et al., 2005) with a maximum number of 116 species and 295 reactions in the gas phase. 110 gas phase reactions and 34 photolysis reactions are explicitly simulated with up-to-date kinetic data in the "troposphere, gas phase, no sulfur, no

20 halogens" mode. The list of reactions can be found in the electronic supplement of Sander et al. (2005), whereby the mode mentioned corresponds to all reactions with the labels Tr and G except the ones also labeled with Cl, F, Br, I or S. Heterogeneous and aqueous phase reactions have been neglected in the present study.

J-values were calculated with an external module (TUV v4.1, Tropospheric

25 Ultraviolet-Visible Model, Madronich and Flocke, 1998) which includes a parameterisation for aerosol (total aerosol optical density OD = 0.34 at λ = 340 nm). The total

ozone column used to scale the ozone profile in the radiative transfer model was fixed to $7.1285 \cdot 10^{18}$ cm^{-2} ($\equiv 265$ DU). Otherwise the TUV settings have been left unchanged compared to Stickler et al. (2006). From measured and modelled $J(NO_2)$ a cloud correction factor (CCF), in large part compensating for cloud and aerosol effects, could be
5 calculated, which was then applied to the model results.

3.2 Specific settings in the Lagrangian mode

The Lagrangian approach can be thought of as a box, not necessarily closed with respect to mass, being traced along a trajectory with constraining parameters (e.g. prescribed trace gas mixing ratios and fluxes, radiation etc.). For the Lagrangian calcula-
10 tion of CO, HCHO and peroxide mixing ratios, the mixing ratios of the long-lived species CO_2 and CH_4 were set to fixed values (377 μmol/mol and 1760 nmol/mol respectively, derived from the NOAA CMDL global trends and the ESRL Global Monitoring Division "Atlantic Ocean Cruise" data at 5° N (autumn 2005), see http://www.cmdl.noaa.gov and http://www.cmdl.noaa.gov/ccgg/iadv/). H_2 was also included with a fixed mixing ratio of
15 563 nmol/mol (Stickler et al., 2006). Since alkanes and alkenes except isoprene were not measured on board the research aircraft during GABRIEL the respective mixing ratios were estimated based on GC-FID measurement results of the Institute of Marine and Atmospheric Research (IMAU) at the University of Utrecht (The Netherlands) obtained during the LBA-CLAIRE98 campaign for the short dry season and in the same
20 region. From these data mixing ratios of 794 pmol/mol (C_2H_6), 83 pmol/mol (C_3H_8), 28 pmol/mol (n-butane + iso-butane) and 84 pmol/mol (C_3H_6) were derived as median values for the altitude range 0–1 km. For C_2H_4 there was no measurement data available for either campaign, so that data obtained during other measurement campaigns in South America had to be considered. Greenberg and Zimmerman (1984) measured
25 mixing ratios of 2.7 nmol/mol directly above the forest canopy in central Brazil. Zimmerman et al. (1988) report a median value of 650 pmol/mol at an altitude of 305 m near Manaus during the dry season (northern hemispheric summer). Since the median flight altitude in the altitudinal range 0–1 km during GABRIEL was about 500 m a.s.l., the lat-

Chemistry, transport and dry deposition of trace gases during GABRIEL

A. Stickler et al.

EGU

ter data obtained during GTE ABLE 2A was taken to be most representative. All values listed here were set to be constant since the sensitivity of the species examined in the present study towards alkanes and alkenes was found to be minor or intermediate (see e.g. Stickler et al. (2006) and Sect. 4.2.1). The above mentioned settings were also used for the "steady state" mode of the box model described in Sect. 3.3.

For CO, HCHO, H_2O_2, organic peroxide, NO, acetone, methanol, isoprene, MVK, H_2O, O_3, OH and HO_2 longitudinal gradients of the median mixing ratios with a resolution of 1° were derived for the whole data set in the altitude range 0–1 km a.s.l. (see e.g. Figs. 2 to 5). In the case of HCHO, the peroxides, NO and HO_x diurnal cycles in time steps of 5000 s, beginning at a local time (LT) of 25 000 s after midnight ($\approx$ 06:55 LT) and ending at 60 000 s after midnight (16:40 LT), were additionally inferred from the measurements. With the exception of NO, OH and HO_2, these diurnal cycles were then "closed" by linearly interpolating the mixing ratios through the nighttime. These three compounds were set to 0 before sunrise (06:00 LT) and after sunset (18:00 LT) to reflect their low nighttime concentration. Diurnal cycles of isoprene, MVK and the photolysis rates were constructed by assuming a proportionality to the sine of the solar elevation angle. The median mixing ratios in the easternmost longitude bin centred at 51.5° W were defined as start values (t=0) for the Lagrangian mode. In the case of species subject to diurnal cycles, the solar dependency was combined with the longitudinal gradient. Starting with the median mixing ratio of the easternmost bin, the air parcel was assumed to travel westward with the measured mean velocity of 5.6 m/s at 0–1 km a.s.l. (measured mean wind direction: $(95 \pm 48)°$). Thus it takes 330 min to cross 1° longitude, approximately equivalent to 60 nm $\approx$ 111 km, close to the equator, and a distance of $\approx$ 4.36° or 484 km is covered in 24 h. From the starting value of the mixing ratio and the local time, the maximum of the diurnal cycle was calculated. The latter was then updated along the trajectory by adding the integrated horizontal gradient of the species over the covered distance. Whenever this combination led to negative values, mainly due to either a strong diurnal cycle (HCHO, HO_2) or a negative longitudinal gradient (H_2O_2), the resulting mixing ratios were set to zero. For the long-

lived trace gases without a diurnal cycle the integrated horizontal gradient was directly added to the starting value of the mixing ratio. The model run was stopped after having traversed a distance of 6° in 33 h.

At the starting point in the centre of the ocean bin (51.5° W) the organic peroxides were assumed to consist solely of CH_3OOH. At the centre points of the bins located further westward over the continent, 60% of the organic peroxide was assumed to be methyl hydroperoxide while the rest was equally distributed over peroxides formed during isoprene oxidation (lumped species ISOOH in MECCA v0.1p) and peroxides formed during MVK oxidation (lumped species MVKOOH). This ensures that the diurnal mean of the CH_3OOH mixing ratio stays roughly constant along the trajectory. In the boundary layer above the rainforest isoprene and its oxidation product MVK are expected to be the major contributors to RO_2 and organic peroxide formation due to their high reactivity and abundance. Sensitivity runs were done with altered partitioning of these 3 peroxides. The mixing ratios of all other organic peroxides existing in the chemical mechanism were consistently set to zero.

Organic nitrates, nitrooxy acetaldehyde (NACA, formed in the model reaction of nitrates from isoprene with OH), HNO_3 and HNO_4 were set to zero in the reference run, too, considering their negligible influence on HCHO (the latter being an ideal indicator for photochemical degradation of VOCs). HNO_3 is only relevant as a source of NO_3 in the model. Nevertheless, several sensitivity runs, including one with freely calculated $NO_z \equiv NO_y - NO_x$, were done for CO to test this hypothesis for the conditions of GABRIEL (Sect. 4.2.1). Finally, formic and acetic acid, not measured during GABRIEL, were neglected in the reference run. This assumption was again checked in the sensitivity study. The mean measured temperature and pressure used for the Lagrangian model runs are 25.9°C and 966 hPa, respectively.

The remainder of the trace gases and the species studied were freely calculated with a time resolution of 5 min. Contrary to Stickler et al. (2006), this includes PAN and MPAN (peroxymethacryloyl nitrate) because of their much shorter chemical lifetime (about 50 min at 25°C Finlayson-Pitts and Pitts, 2000) compared to the upper

troposphere.

Each complete model simulation consisted of 57 single model runs with slightly changed initial conditions following the "equivalent longitude" concept introduced in Stickler et al. (2006):

$$\text{lon}_{\text{eq.}} = \overline{(\text{local time} - \text{model time})} \cdot \frac{360°}{24 \cdot 3600\text{s}} + \Delta\text{lon}_{\text{eq.}} \tag{1}$$

where

$$\Delta\text{lon}_{\text{eq.}} = k \cdot 1.25°$$

and

$$k = -\sigma(\text{local time}) \cdot \frac{360}{24 \cdot 3600\text{s}} \cdot 1.25, \ldots, +\sigma \ldots$$

For this study, the equivalent longitude was calculated as $(12.4 \pm k \cdot 1.25)°$, $k = 0 \ldots 28$, reflecting the 1σ empirical standard deviation of the local time for all flight data below 1 km altitude in the pure ocean bin between 51° W and 52° W. This corresponds to a mean local time of 46 176 s after midnight or circa 12:50 LT. As no clear longitudinal gradient of the radiation measurements could be detected, this time was allocated to the arithmetic mean of all $J(NO_2)$ values measured below 1 km. The diurnal cycle of the J-values was then calculated as in Stickler et al. (2006), using

$$\overline{|43\,200\text{ s} - \text{local time}|} = 35\,411\text{ s} \tag{2}$$

and a mean latitude of 4.672° for the calculation of the diurnal maximum, and assuming a proportionality with the sine of the solar elevation angle. To be able to interpret the model results, arithmetic means of the 57 values of the examined variables computed at a model time of 24 h were calculated. This procedure optimises the comparability of the model results and the measurements.

3.3 Specific settings in the "steady state" mode

In the case of HCHO and H_2O_2 (only over the ocean) the box model was also used in a "steady state" mode allowing for the assessment of the chemical equilibrium of shorter lived species like HCHO, or in an environment as for the investigation of the dry deposition of H_2O_2 in the relatively aged air masses arriving from the east over the ocean.

For this purpose 6 segments from the 2 flights (G04 and G07) covering the ocean and the continental region in the eastern part of the total operating area (see Fig. 1) were selected. These 2 flights offered the advantage that each included 3 BL flight legs, one above the ocean and two above the rainforest, and the flight paths were nearly identical. The flight legs were termed "Gxxa", "Gxxb" and "Gxxc" with the flight number xx and a, b, c for the eastern (ocean), middle (rainforest) and western (rainforest) flight leg.

For each case the mean equivalent longitude, Eq. (2) and the parameter k were evaluated. As the studied flight segments were quite short, generally about 15 min, the absolute value of k was always less than 3, equivalent to a variation of ± 15 min in local time. Accordingly, the variation of the initial boundary conditions could be turned down as no significant nonlinear averaging effects are expected (see discussion in Stickler et al., 2006).

Mean values of static air pressure, temperature, latitude and the photolysis rates were calculated for each case. Additionally, the average mixing ratios of the measured trace gases were evaluated for the respective time periods. By visual inspection of all time series, single pollution "plumes" were ruled out. There was only one event during flight G07 when NO volume mixing ratios showed a strong rise and several peaks over the ocean for at least 15 min without a corresponding signal in CO or other species. This part of the measurements has been excluded from the present study. In the case of NO median instead of mean mixing ratios were implemented because sharp peaks in the NO data do not adequately represent the chemical conditions above the ocean

and the rainforest environment, typically poor in NO_x, and would lead to an artificial overestimation of HCHO due to the strong sensitivity of this compound towards NO (Stickler et al., 2006).

In the case of H_2O there was no data available for flight G07 so that the mixing ratios were assumed to be the same in the eastern, middle and western part of the longitudinal transects as during flight G04. This assumption does not significantly influence the results of the study as H_2O does not play a major role for the chemistry in the box model when OH and HO_2 are constrained by measurements. Radiation measurements were not available for G07c so that photolysis rates were assumed to be the same as in case G07b. Since methanol, acetone and isoprene were not measured during G07c, it was assumed that

$$\frac{x_s(\text{G07b})}{x_s(\text{G07c})} = \frac{x_s(\text{G04b})}{x_s(\text{G04c})} \tag{3}$$

with the mixing ratio x of the species s involved. This seems reasonable because segments G04b and G04c are located in the same region as G07b and G07c, respectively. Finally, for flight G07 only total peroxide data is available. From this data and the BL ratio of the medians H_2O_2/org. peroxide resolved in longitudinal bins of 1° for the whole campaign data, the values were inferred assuming these ratios were also valid during flight G07. The organic peroxides were subdivided into CH_3OOH, ISOOH and MVKOOH by assuming measured organic peroxide over the ocean to consist only of CH_3OOH and keeping its mixing ratio constant over land, similar with the procedure for the Lagrangian mode. As in the Lagrangian case sensitivity runs were done with altered partitioning. For isoprene, MVK, Cl, OH and HO_2 diurnal cycles identical to the ones described for the Lagrangian mode were prescribed. The one for NO was changed for the oceanic segments such that the morning peak in the median of all BL data of about 50 pmol/mol was filtered out, since this peak is a typical feature produced by the lifting of the BL over land and the photolysis of NO_2 having accumulated during nighttime. The concentrations of all other measured species were kept constant. The model run was stopped after the daily change of HCHO had reached less than 0.01%

($\approx$ 30–50 days in the case of HCHO).

3.4 Determination of the BL height

For all model runs explicitly including the effect of dry deposition it was necessary to obtain an estimate of the BL height. These include the "steady state" and Lagrangian calculations of HCHO, the runs for the assessment of the H_2O_2 dry deposition veloc-ity and the Lagrangian run calculating the time development of the organic peroxides along the examined trajectory.

This estimate is based on the diagnostic BL height from simulations with a single-column model (SCM) version of the global 3-D chemistry-climate model ECHAM4 (Roeckner et al., 1996, 1999; Ganzeveld et al., 2002, 2006a,b). The 1-D SCM has also been applied to study more precisely the BL chemistry during the GABRIEL cam-paign[2]. The trajectory of the SCM starting at 45° W 4.5° N shows that the BL height over the ocean is roughly constant over time so that a fixed value of 570 m (mean BL height for 50–51° W) was chosen. As expected, above land the model results show a strong diurnal variation with a minimum BL height during nighttime ($\approx$60–120 m) and a maximum during daytime ($\approx$1100 m). Consequently, a diurnal cycle was derived by fitting a 3rd order polynomial to the data. According to these results the BL height over land exceeded 500 m between 08:45 LT and 18:15 LT.

In the 6 cases described above, the flight altitudes in the BL were about: 330 m (G04a), 500–510 m (G04b), 385–660 m (G04c), 325 m (G07a), 375–490 m (G07b) and 380–485 m (G07c). Flight G04 was conducted in the early afternoon at a time of the day when the BL height is predicted to be at maximum. In contrast, flight G07 was performed in the morning hours. The earliest local time during the measurements be-tween 0–1 km a.s.l. over land is (08:55 LT ±5 min). The aircraft was therefore clearly located in the BL during flight G04 when flying the segments examined with the "steady state" model, while for flight G07 it cannot be ruled out that the aircraft was situated

---

[2]Ganzeveld et al. (2007), Atmos. Chem. Phys. Discuss., in preparation, 2007.

just above the growing BL and inside the residual BL. Nevertheless, low ozone mixing ratios of <15 nmol/mol, similar to the ones measured in the marine BL on the same day compared to 27–50 nmol/mol and higher at ≈ 1–3 km a.s.l. argue against this. Additionally, sharp peaks in the CO data in the range 2–3 km point towards a relatively

5 strong inversion layer and the NO data shows generally enhanced mixing ratios with peaks up to 290 (G07b) and 150 pmol/mol (G07c), respectively. Finally, the flight altitude is referenced to the sea and not the land surface so that it is an upper limit of the altitude above ground. Hence, from the synopsis of all information available it appears likely that these measurements were also taken in the BL. For the Lagrangian studies

10 using all flight data, the predominant part of the data in the altitude range 0–1 km were taken in the BL as 80% of the flights took place at noon or in the afternoon before sunset.

3.5 HCHO deposition velocity

To test the representation of the organic chemistry and to cross-check the box model

15 results for CO (see Sect. 4), "steady state" and Lagrangian model runs for HCHO were performed. In the BL dry deposition has to be included for HCHO, even though its chemical lifetime can be relatively short depending on the solar radiation and the OH radical concentration. The explicitly calculated dry deposition velocity for a reference altitude of 34 m above ground from the 1-D SCM was taken as best guess for this

20 parameter, resulting in a constant value of v_d(HCHO)=0.357 cm/s above the ocean and a diurnal cycle above the rainforest (minimum 0.05 cm/s, maximum 1.1 cm/s), derived as 3rd order polynomial fit of the SCM data. The SCM includes the turbulent transfer to the surface, molecular diffusion calculated explicitly from the SCM's micrometeorology and uptake by leaf stomata and other substrates including the soil, wet and dry cuticula

25 and oceans. The estimated uptake resistances are based on solubility and reactivity of the trace gases.

3.6 Halogen chemistry

In the oceanic segments of the "steady state" model runs, chlorine radical chemistry was included to test the sensitivity of formaldehyde formation to halogen chemistry in the tropical marine BL. At Cl concentrations of $1 \cdot 10^4$ cm^{-3} the chemical lifetime of alkanes and alkynes towards this species is of the same order as the one towards OH radicals ($1 \cdot 10^6$ cm^{-3}) (Finlayson-Pitts and Pitts, 2000). Results of measurements and estimates of chlorine radical concentrations in the marine BL of the tropics as well as the midlatitudes range two orders of magnitude (($0.25...30) \cdot 10^4$ cm^{-3}, Singh et al., 1996; Wingenter et al., 1996; Lowe et al., 1999; von Glasow et al., 2002; Chang et al., 2004; Platt et al., 2004). Therefore a Cl concentration of $1 \cdot 10^4$ cm^{-3} was implemented in the reference run while additional sensitivity runs with the upper and lower limits were performed.

4 Results and discussion

4.1 Measured longitudinal gradients

The mixing ratios of several trace gases measured show longitudinal gradients between 0–1 km a.s.l. generally with an increase from east to west, i.e. from the ocean to the rainforest. Analysing longitudinal transects of the median mixing ratios for the whole data set in the BL we find the following tendencies:

- For CO (Fig. 2) a clear and significant east-west increase is observed: values generally below 100 nmol/mol are found in the BL over the easternmost ocean bin (50% of all measured values lie between 80 and 95 nmol/mol) while higher values were measured over land (up to 115–130 nmol/mol in the westernmost bin). The horizontal CO gradient is about twice as strong (30 (nmol/mol) / 560 km $\approx$ 54 pmol/mol km^{-1}) compared to LBA-CLAIRE98 (29 pmol/mol km^{-1} Williams et al., 2001a).

- For O_3 no unequivocal tendency was found for the mean, but again for the median mixing ratios (Fig. 3), mainly due to low outliers in the westernmost bin over the rainforest. The mixing ratios of this trace gas are characterised by a relatively low median of 14 nmol/mol in the easternmost bin (ocean), whereas significantly higher medians were found in the west (up to 19.5 nmol/mol). A region that stands out for O_3 (and also NO and perhaps H_2O_2) is the coastal region of French Guyana (transitions from ocean to land were generally located around 52° W) with a median of 18.5 nmol/mol and highly variable mixing ratios. The fact that 10% of the data lie above 29 nmol/mol probably indicates an anthropogenic influence in this relatively densely populated region compared to the practically uninhabited rainforest regions.

- Despite the relatively low precision of the measurements of 25% at 1.0 nmol/mol, a significant tendency can be seen for HCHO with median mixing ratios from 429 pmol/mol in the pure ocean bin to 1873 pmol/mol in the westernmost bin over the rainforest (Fig. 4).

- Organic peroxides (Fig. 5) show again a distinct increase of the median mixing ratio with lowest values over the ocean (594 pmol/mol), steadily increasing to 1088 pmol/mol above the western rainforest area.

Median instead of mean values were used to filter sharp peaks and outliers visible e.g. in the NO data as a result of local sources of the trace gases, not considered in this study.

4.2 CO

Figure 6 shows the expected CO mixing ratios along the trajectories, i.e. the mixing ratios obtained by superimposing the measured longitudinal gradients and diurnal cycles as described in Sect. 3.2, and taking into account the different starting times according to the varying k values ($\approx$ 38 000–55 000 s after midnight equivalent to 10:30–

15:15 LT). The measured median CO mixing ratio at 51.5° W, the starting mixing ratio for both the expected and the modelled CO along the trajectories, is 85.6 nmol/mol. The measured (and expected) mixing ratio at 55.86° W corresponding to 24 h transport time is 109.8 nmol/mol. In contrast to this the model results of the reference run give an average of only 88.3 nmol/mol (Fig. 7).

While the expected difference of the starting and ending mixing ratios is ΔCO=24.2 nmol/mol, corresponding to a longitudinal gradient of 50.0 pmol/mol km^{-1}, the model indicates only an increase of ΔCO=2.7 nmol/mol or 5.6 pmol/mol km^{-1} by chemical sources. Table 2 presents the analysis of all three flights with available CO measurements conducted towards the east in the BL over ocean and rainforest. This analysis suggests longitudinal gradients of CO between 16–48 pmol/mol km^{-1}, being variable and rather smaller than the one derived from the median of all flights, but still significantly larger than the value 5.6 pmol/mol km^{-1} predicted by the Lagrangian model without FT entrainment and soil sources. As in the study by Williams et al. (2001a) of measurements during the LBA-CLAIRE campaign, the CO mixing ratios in the BL over the ocean exhibit quite strong day-to-day variability ($\approx$ 82–102 nmol/mol), stronger than over the rainforest (105.6–110.7 nmol/mol), and indicating changes in the composition of air advected to the coast.

To make sure that the calculated gradient is not artificially enhanced by these changing "background" conditions, we searched for an approximately "true" Lagrangian case and found one between different legs of flight G03 and G04. The measurements in the easternmost part of the eastern boundary layer leg during G03 (06/10/2005) and the western boundary layer leg during G04 (07/10/2005) are closest to a "real" Lagrangian event, with the projected position of the air mass during G03 about 100 km west of the flight track during G04. For this case ΔCO $\approx$7.7 nmol/mol in 22 h transport time corresponding to a gradient of 17.5 pmol/mol km^{-1}, similar to the smallest gradient calculated before. Again, it is significantly larger than in the model, confirming the earlier results.

Provided that the chemistry in the mechanism is represented correctly these results

imply that there must be other sources significantly influencing CO. In principle these can be a) direct emission of CO, e.g. by biomass burning or from the soil, or b) mixing-in from above the BL of free tropospheric air richer in CO or c) other chemical sources not in the model could be present, e.g. terpenes/sesquiterpenes.

4.2.1 Sensitivity study for the chemical production of CO

To ensure the robustness of our results with respect to the chemistry a sensitivity study was conducted. A large number of parameters was changed with the reference run generally being the starting point for the variation of the parameters. The only exception is the variation of organic peroxides. To determine the sensitivity of CO towards the latter, a reference run without organic peroxides was made. Table 3 shows the results of these calculations.

A high sensitivity of CO mixing ratios in the Lagrangian model towards NO_3, NO, HCHO, MVK, MVKOOH and nitrooxy acetaldehyde is revealed in this data. Absolute sensitivities [(nmol/mol)/(nmol/mol)] towards peroxides from acetone, butane, ethane, MEK and towards nitrates from the isoprene oxidation, propene, acetaldehyde, hydroxy hydroperoxides from propene, hydroxy acetone, isoprene, MEK, organic nitrates from higher alkyl nitrates (plus $C_3H_6+NO_3$) and ethene are intermediate, while the calculated sensitivities towards methyl hydroperoxide, acetic acid, nitric acid, nitrate from propane, peroxide from isoprene and from propane oxidation are small. For formic acid no sensitivity run was necessary due to the fact that this species is only important for HO_x partitioning in the model which is prescribed by the measurements.

The test value of 5 nmol/mol for the sensitivity run of $CH_3C(O)OH$ was chosen following Helas et al. (1992) who report values of up to 3–4 nmol/mol measured in northern Congo. For $CH_3 CHO$ an upper limit of 5 nmol/mol was estimated from ranges of 1–18 nmol/mol in urban, 0.1–4 nmol/mol in rural and 0.1–1 nmol/mol in remote areas given by Finlayson-Pitts and Pitts (2000) and from a value of 0.129 nmol/mol reported by Jacob and Wofsy (1990) for the Brazilian rainforest during the wet season. The sensitivity towards HNO_3, organic nitrates from higher alkyl nitrates and from the reaction

of C_3H_6 with NO_3 (ONIT), and i-propyl nitrate was tested with mixing ratios of 0.25, 0.05 and 0.05 nmol/mol, respectively, derived as upper limits from ABLE measurements and model results by Jacob and Wofsy (1988, 1990). A model run with freely calculated NO_z gave maximum mixing ratios of 125 pmol/mol (HNO_3), 0.1 pmol/mol ($C_3H_7ONO_2$),
5 6 pmol/mol (ONIT), 183 pmol/mol (NACA) and 285 pmol/mol (nitrate from isoprene oxidation, ISON), clearly smaller than the values used for the sensitivity test (see below). When calculated freely the levels of the mixing ratios of MEK, hydroxy acetone and methyl glyoxal ($CH_3C(O)CH_2OH$) are at about 2 pmol/mol, 1.3 nmol/mol and 0–300 pmol/mol. Sensitivity runs were performed with mixing ratios of 1.8 nmol/mol and
10 606 pmol/mol for MEK and hydroxy acetone (mixing ratios reported for the BL during LBA-CLAIRE in Williams et al., 2001b). If the identification of m73 with MEK proposed in that study is correct, the striking difference between modelled and measured MEK suggests that direct emissions of MEK are much more important than its photochemical production. In the case of methyl glyoxal the chemical lifetime is so short (visible in
15 the diurnal cycle) that the chemistry is approximated by steady state.

The at a first glance surprisingly low sensitivity of CO towards isoprene and CH_3OOH in the model can be explained by the fixed intermediate (HCHO and MVK) mixing ratios via which the oxidation of these two species primarily proceeds (see e.g. Stickler et al., 2006). The high sensitivity towards NO_3 must be caused by a generally higher
20 formation rate of the peroxyacetyl radical by the reaction sequence

$$C_2H_5O_2 + NO_3 \rightarrow CH_3CHO + HO_2 + NO_2 \tag{R1}$$

$$CH_3CHO + NO_3 \xrightarrow{O_2} CH_3C(O)OO + HNO_3 \tag{R2}$$

The formed radical can further react with NO_3, producing CH_3O_2 and CO_2, thus partly bypassing CO as intermediate:

25 $$CH_3C(O)OO + NO_3 \rightarrow CH_3O_2 + NO_2 + CO_2 \tag{R3}$$

At the same time the equilibrium of the reaction

$$CH_3C(O)OO + NO_2 \rightleftharpoons PAN \tag{R4}$$

Chemistry, transport and dry deposition of trace gases during GABRIEL

A. Stickler et al.

is shifted towards the reservoir species peroxyacetyl nitrate due to the fact that the NO_2 mixing ratios are much higher in this case compared to the reference run and induced by the three reactions

$$CH_3O_2+NO_3 \rightarrow HCHO+HO_2+NO_2 \tag{R5}$$

$$C_2H_5O_2+NO_3 \rightarrow CH_3CHO+HO_2+NO_2 \tag{R6}$$

and R3, further slowing down the CO production. Interestingly, the sensitivity of CO towards NACA and ISON is not found to be negligible, as expected initially. This can be rationalised by considering that the study by Stickler et al. (2006) suggested that, in the upper troposphere, these compounds would accumulate to unrealistically high mixing ratios in a simple steady state box model. Therefore it seemed reasonable in that study to neglect them without suffering a significant impact on the HCHO or CO budget. Contrarily, the present study examines boundary layer chemistry in a region strongly affected by precursor emissions of the two species, so that the potential influence of the latter on CO has to be estimated at least in the context of a sensitivity study. CO shows no sensitivity at all towards ISOOH in the model. This can be understood by taking into consideration that ISOOH reacts with OH to form MVK and photolyses to give MVK, HCHO, HO_2 and OH as products, all compounds prescribed by the measurements. Thus changing the partitioning of the organic peroxide in favour of ISOOH leads to a decrease in CO.

Allowing for the examined realistic variations caused by measurement errors and other uncertainties we can conclude that the uncertainties connected to the measurements/estimates of the different precursors of CO are not large enough to explain the discrepancy between the measured and modelled longitudinal gradient.

4.2.2 Biomass burning and surface sources

ABBA (Automated Biomass Burning Algorithm) fire maps prepared from GOES-12 satellite images of South America (Cooperative Institute for Meteorological Satel-

lite Studies (CIMSS), http://cimss.ssec.wisc.edu/goes/burn/wfabba.html) show no evidence of forest fires or significant biomass burning directly in the region where the measurements took place (Guyanas). Biomass burning was generally only detected south or west of this region in deforested parts of the Guyana Highlands in northern Brazil south of the Surinamese border, in the region of Boa Vista (Roraima, Brazil) and especially in eastern Venezuela (region around Ciudad Guayana). In these cases the wind direction in the BL precludes a possible influence of the fires on our measurements. An exception is 15 October 2005 (flight G10) when fire activity was observed along the coast of French Guyana and in northern Guyana. Nevertheless, no influence of these fires on the CO mixing ratio can be seen in the BL data obtained over Suriname, i.e. in the form of enhanced volume mixing ratios. On the contrary the mixing ratios measured over the western part of Suriname are higher than the ones from the eastern part of the country, being closer to the fires in French Guyana, thus confirming the general east-west gradient. Visual observations of the operators on board the aircraft indicate only one fly by past a biomass burning plume over French Guyana at 16:14 UTC on 7 October 2005 (G04), not reflected in the CO data, and the crossing of a smoke plume at about 16:20 UTC on 8 October 2005 (G05), matching a sharp peak up to almost 160 nmol/mol.

In some cases the BL CO mixing ratios (75–135 nmol/mol, peaks during flights G05 and G08 up to 170 nmol/mol) were comparable or higher than the mixing ratios in the FT. During flights G03, G04, G05 (only partly), G07 and G08 significantly higher mixing ratios were detected above the BL between 2–3 km altitude though (no CO data is available for flight G06). During G03 a maximum CO mixing ratio was found at an altitude of 2500–3000 m a.s.l. with maximum differences of $\approx$ 6–20 nmol/mol between BL and FT mixing ratios. Yet the average difference of the layers 0–1 and 1–3 km a.s.l. is only 1.6 nmol/mol as the mixing ratio decreases again above this relatively thin layer of enhanced CO. For G04 a much more elevated mean difference of these layers of 18 nmol/mol was found, whereas the enhancement, at least over the continent, was again concentrated in a thin layer at about 2500 m a.s.l.. CO

Chemistry, transport and dry deposition of trace gases during GABRIEL

A. Stickler et al.

data from G07 shows peaks up to 270 nmol/mol at about 3 km altitude and data from G08 exhibits a maximum of approximately 140 nmol/mol at about 2 km altitude. Fire maps (see also MODIS data on http://rapidfire.sci.gsfc.nasa.gov/firemaps), trajectory (KNMI/ECMWF and NOAA, http://www.arl.noaa.gov/ready/hysplit4.html) as well as 3-
5 D Chemistry Transport Model (CTM) calculations (MATCH-MPIC; Lawrence, private communication) suggest that these enhancements in CO could originate from biomass burning in western or southern central Africa and partly also in other parts of South America south of the Guyanas. MODIS fire maps for this period show fires e.g. in eastern Brazil, Mauretania/Mali and Congo/western and southern Democratic Repub-
10 lic of Congo/Angola/Sambia. Chatfield et al. (1998) have proposed a mechanism for the intercontinental export of CO in the middle troposphere up to 5.5 km altitude from Africa to South America based on deep mixing from the BL up to altitudes of 2.5–5 km over Africa and lofting over the monsoon inflow of the equatorial African coast, termed the "Great African CO Plume". They report a very intense transport of CO along this
15 pathway with alternate phases of higher and lower mixing ratios travelling slowly from east to west in October 1994. In that year the main transport took place further south at about 5° S though.

Several authors have reported investigations of carbon monoxide fluxes from different soil types. Sanhueza et al. (1994) report measurements of this flux from nonper-
20 turbed savannah grasslands in Venezuela obtained with an enclosed chamber technique, and find that this soil type is a net source of CO ($3.4 \cdot 10^{10} \text{cm}^{-2} \text{s}^{-1}$). The same technique had already been used by Conrad and Seiler (1985) for measurements in Spain, South Africa and the Namibian desert. The maximum flux they derived was $\approx 1.3 \cdot 10^{11} \text{cm}^{-2} \text{s}^{-1}$ under midlatitude conditions with dry, carbon-rich soil in Ger-
25 many although the study predicts probably even higher fluxes from warm and carbon-rich soils as in the rainforests. Kirchhoff and Marinho (1990) estimated a CO flux of $4 \cdot 10^{11} \text{cm}^{-2} \text{s}^{-1}$ from the Amazonian rainforest during the wet season by means of vertical gradient measurements at a tower near Manaus. A comparable value for the mean emission flux of $\approx 4.36 \cdot 10^{11} \text{cm}^{-2} \text{s}^{-1}$ can be obtained from the model study of Tao and

Jain ([2005](#)) by converting the 31.7 Tg C emitted in the form of CO by the global tropical evergreen forests ($\approx$12.1$\cdot$10^6 km^2 according to [Loveland et al., 2000](#)) into cm^{-2} s^{-1}. Additionally, field and laboratory studies suggest that CO is not only emitted by dead plant matter but also by live leaves ([Scharffe et al., 1990](#); [Tarr et al., 1995](#)). [Scharffe](#) et al. ([1990](#)) estimated a CO flux from termites and vegetation of 5$\cdot$10^{10} cm^{-2} s^{-1} in a scrub grass savannah in Venezuela. However, one should keep in mind that these flux estimates are associated with relatively large uncertainties.

When taking into account a height of the mixed BL of 1100 m (see Sect. [3.4](#)) and the concentration of air molecules of 2.34$\cdot$10^{19} cm^{-3} at 966 hPa, the four specified measured fluxes result in a 24 h increase in the CO BL mixing ratio of 1.1 nmol/mol, 4.3 nmol/mol, 13.4 nmol/mol and 1.7 nmol/mol respectively. Only the largest of these values would, together with photochemical production from VOCs, be sufficient to explain the lower half of the range of observed longitudinal gradients. To match the full range of these gradients a CO emission flux of 1.5$\cdot$10^{11} cm^{-2} s^{-1} up to 6.1$\cdot$10^{11} cm^{-2} s^{-1} is necessary.

To summarise, it is conceivable that CO soil emissions contribute to the budget of CO in the BL over the tropical rainforest and possibly even regionally outbalance the importance of photochemistry for this trace gas. Nevertheless, it remains questionable if the strong horizontal gradient of the CO mixing ratio can be fully explained by a combination of photochemical processes and soil emissions alone.

4.2.3 Entrainment of air from the free troposphere into the planetary boundary layer

Entrainment of FT air richer in CO into the BL is another possibility to explain the observed strong longitudinal CO gradient. We assessed the upper limit of the 24 h average entrainment rate using the mean difference of the mixing ratios in the BL and in the FT, both defined as above as the layers between 0–1 and 1–3 km a.s.l., respectively. This calculation was done for flights G03 and G04, the flights which represent the "Lagrangian" case as described in Sect. [4.2](#).

As mentioned earlier the longitudinal gradient derived for this case, which can be re-

garded as the best estimate for the "true" gradient without changes in background CO, was determined to be ≈ 17.5 pmol/mol km^{-1} while the model results without emissions and entrainment indicated a gradient of ≈ 5.6 pmol/mol km^{-1}. We estimate an upper limit of the mean entrainment rate by assuming that the difference of these values (i.e. 11.9 pmol/mol km^{-1}) is caused by mixing-in of air from the FT with a CO mixing ratio 1.6 and 18 nmol/mol higher than in the BL. The latter are the average differences between BL and FT mixing ratios (Δx_{FT-BL}) during flights G03 and G04 respectively (see Sect. 4.2.2). At a mean wind speed of 5.6 m/s the gradient of 11.9 pmol/mol km^{-1} is equivalent to a temporal increase $\Delta x_{BL}/\Delta t \approx 239$ pmol/mol h^{-1}, larger than the average predicted chemical production rate. If the differences in the mixing ratios are assumed constant, the mean fractional entrainment rate ER can be expressed as

$$ER = \frac{\Delta x_{BL}/\Delta t}{\Delta x_{FT-BL}} \tag{4}$$

i.e. a fraction ER of the BL air is exchanged with FT air per unit of time. In our case this calculation leads to $ER \approx 0.15$ h^{-1} (G03) and $ER \approx 0.01$ h^{-1} (G04). The discrepancy between the two values for G03 and G04, which stem from the different BL-FT gradients of the CO mixing ratios, is reflected in the vertical gradients of the peroxide mixing ratios during these flights. The latter show a similar behaviour during these two days with a weak gradient during G03 pointing at a well mixed lower troposphere, and a strong gradient during G04 indicating a layered structure with minor vertical exchange. Consequently, the first value is taken as an upper limit for the 24 h mean entrainment rate.

4.3 HCHO

4.3.1 Steady state model

The steady state model described in Sect. 3.3 was applied to predict HCHO mixing ratios in the six cases defined there. This was done to cross-check the results obtained

with the Lagrangian CO model, and particularly to investigate if some organic precursors are missing in the chemical mechanism, which could have been another explanation for the too low predicted CO mixing ratio. As mentioned earlier, dry deposition of HCHO was accounted for in this model by using the deposition velocity calculated explicitly with a 1-D SCM and the diagnostic BL height from ECHAM4. Entrainment was not included in these calculations. Instead an upper limit for the daytime entrainment rate was deduced from a Lagrangian model run (Sect. 4.3.3). The arithmetic means of the measured HCHO mixing ratios together with model results are listed in Table 4.

The results show that, contrary to the findings for CO, the mixing ratios of HCHO are partly drastically overestimated by the "steady state" model in the reference case. Only an unlikely combination of several reduced parameters leads to a better agreement of measurement and model results (OH –25%, NO –5 pmol/mol, Cl –75%, v_d(HCHO) = v_d(HNO$_3$)). Here, the explicitly calculated v_d(HCHO) from the 1-D SCM is reflecting a significant role of surface removal processes, indicated by a maximum v_d smaller than the turbulent exchange velocity. v_d(HNO$_3$), on the other hand, is removed very efficiently at the surface in the model. By performing this analysis, we have assessed the impact of an upper limit removal efficiency. The sensitivity towards chlorine radicals is minor in the low range ($(0.25...1) \cdot 10^4 \, \text{cm}^{-3}$) whereas it gradually increases in the higher concentration range ($(1...30) \cdot 10^4 \, \text{cm}^{-3}$). Assuming normally distributed and statistically independent variables the necessity of the combination of two parameter modifications with $\Delta_1 \leq -0.5\sigma$ and $\Delta_2 \leq -1\sigma$ alone corresponds to a probability of

$$
P = \prod_{k=1}^{2} \frac{1}{2} \left(1 - 2 \cdot \int_{\Delta_k}^{0} f(x) dx \right)
$$

$$
= \frac{1}{4} \prod_{k=1}^{2} \left(1 - 2 \cdot F(x) \big|_{\Delta_k}^{0} \right) < 0.05 \tag{5}
$$

with the standard Gaussian distribution function

$$f(x) = \frac{1}{\sqrt{2\pi}} \exp\left[-\frac{1}{2}x^2\right]$$

its primitive

$$F(x) = \int f(x)dx$$

and

$$F(x)\big|_{-1\sigma}^0 = 0.3413, \; F(x)\big|_{-0.5\sigma}^0 = 0.1915$$

(Schönwiese, 1992)

so that the model-measurement discrepancy is significant on a 95% basis. Additionally, the calculated MEK and acetaldehyde mixing ratios in the model are at the lower end of measurements during LBA-CLAIRE and other campaigns. This outcome precludes a deficiency in the chemical mechanism as the reason for the discrepancy in the case of CO, at least for all species being oxidised via HCHO to form CO and not directly forming CO by circumventing HCHO as intermediate.

Since wet deposition is not likely to be very important (Henry constant k_H(HCHO) $=6 \cdot 10^3$ M/atm at $T=273.15$ K, $p=1013.25$ hPa, http://www.mpch-mainz.mpg.de/~sander/res/henry.html) and the effect of dry deposition is limited by the deposition velocity of HNO_3, this fact points again at the possible role of exchange of boundary layer air with the FT (containing less HCHO), even on the relatively short time scale of the HCHO lifetime, which is 50–100 min during daylight according to the steady state model. The only other possibility to bring model results and measurements closer together would be heterogeneous removal of HCHO on aerosol particles. However, this seems unlikely taking into consideration the result of de Reus et al. (2005), who found no significant influence of heavy aerosol loading on HCHO in a Saharan dust plume. A haze layer above the rainforest was noticed several times by the operators on board the

EGU

aircraft though. Unfortunately, no quantitative aerosol measurements were performed during the GABRIEL campaign. In summary, it appears probable that the lack of entrainment from the free troposphere in the reference run, perhaps in combination with an underestimation of the dry deposition of HCHO by the 1-D SCM, is responsible for the overprediction of HCHO. Entrainment alone with the rate computed in Sect. 4.2.3 cannot account for the whole difference during daylight, as will be seen in Sect. 4.3.3.

4.3.2 Lagrangian model

To underpin the results of the steady state model an additional Lagrangian model run for HCHO was realised. The CO model using the data from all flights was modified such that HCHO instead of CO could be freely calculated. Again HCHO deposition was introduced as described in Sect. 3.5. Halogen chemistry was neglected since the steady state calculations indicated that Cl did not play a significant role in the HCHO budget in the marine BL at concentrations up to $1 \cdot 10^4$ cm^{-3}. This is due to the facts that a) the Cl chemistry of non-methane organic compounds (NMOCs) except HCHO and CH_3OOH is not included in MECCA v0.1p, that b) inclusion of Cl chemistry seems to have similar effects on the production and the destruction terms of HCHO and that c) all measured species except HCHO are constrained by the observations.

These computations yield a mean HCHO mixing ratio of 2288 pmol/mol after 24 h transport time for all 57 runs of the model compared to 1498 pmol/mol deduced from a linear longitudinal interpolation of the measured medians combined with the observed diurnal cycle (see Figs. 8 and 9). The model predicts much higher formaldehyde than was measured, substantiating the earlier conclusions.

4.3.3 Lower limit for maximum daytime entrainment

A lower limit for the maximum daytime entrainment rate from the FT into the BL has been determined using the given modelled and measured HCHO mixing ratios and the longitude dependent HCHO mean mixing ratio at 1–3 km altitude for all flights. It is

Chemistry, transport and dry deposition of trace gases during GABRIEL

A. Stickler et al.

Title Page

Abstract | Introduction

Conclusions | References

Tables | Figures

◀ | ▶|

◀ | ▶

Back | Close

Full Screen / Esc

Printer-friendly Version

Interactive Discussion

EGU

assumed that the chemical lifetime

$$\tau_{HCHO,daytime}(\approx 1h) \overset{!}{=} \tau_{entrain} \tag{6}$$

where

$$\tau_{entrain} := \frac{HCHO_{meas\ BL} - HCHO_{model,\ 24\ h}}{\left(HCHO_{meas\ FT} - HCHO_{model,\ 24\ h}\right) \cdot ER}$$

so that the influence of the entrainment on the HCHO mixing ratio would be equal to that of the chemistry. Here $HCHO_{meas\ BL}$ is the linearly interpolated measured median of the HCHO mixing ratio at 55.86° W, $HCHO_{model,\ 24\ h}$ is the model predicted mixing ratio in the BL after 24 h runtime and $HCHO_{meas\ FT}$ is the mean measured mixing ratio in the above defined FT. This calculation is based on the idea that only mixing processes with a characteristic mixing time of the same magnitude or smaller than the chemical lifetime of the examined species will strongly influence the mixing ratio of the species. Evaluating the equation leads to $\max(ER_{daytime}) > 0.549\ h^{-1}$.

A second estimate for this parameter has been obtained from the steady state model using the mean daylight hour difference of the HCHO mixing ratios in the BL and in the FT during flight G04 and the steady state mixing ratio calculated for case G04c. This results in $\max(ER_{daytime}) > 0.689\ h^{-1}$.

In conclusion, the ER values derived from the HCHO measurements are clearly higher than the 24 h averages derived from the CO data and imply effective mixing-in of FT air into the PBL on timescales smaller than the lifetime of HCHO during daylight. This argument is valid if entrainment is considered to be the only loss process besides gas phase chemistry and dry deposition. On the other hand, the significant vertical gradients in CO between the BL and the FT observed during several flights argue against a continuous efficient daytime entrainment. As noted before, the calculation of the entrainment rate makes use of the HCHO dry deposition rate computed explicitly with a 1-D SCM. The latter is similar to the predicted dry deposition rate of HNO_3 over the ocean but much smaller over land (maximum of the diurnal cycle of 1.1 cm/s compared to ≈ 2.6 cm/s). Furthermore, the model-estimated dry deposition of

Chemistry, transport and dry deposition of trace gases during GABRIEL

A. Stickler et al.

EGU

HCHO generally seems to be relatively small compared to values found e.g. by Krinke (1999) for a forest in Germany, particularly when allowing for the extrapolated effect of a higher temperature in Suriname. More efficient dry deposition would lead to a smaller estimated ER. Another possibility to bring the values derived from CO and HCHO analysis closer to each other would be possible heterogeneous loss processes of HCHO on aerosol particles.

4.4 H$_2$O$_2$

4.4.1 Dry deposition velocity over the ocean

The average dry deposition velocity $v_d(H_2O_2)$ over the ocean has been assessed using the steady state model. v_d was varied so that measured and modelled hydrogen peroxide match. Entrainment was included in the model with a constant rate $ER=0.12$ h^{-1}. The initial and boundary conditions were taken from case G04a and G07a (eastern sector) with mean mixing ratios in the FT of ≈ 4.3 nmol/mol and ≈ 1.0 nmol/mol respectively (51.5–52.5° W, G04 and G07). The latter mixing ratio was deduced from the total peroxides as described in Sect. 3.3. This corresponds to "positive" (concentrating) entrainment in the first and "negative" (diluting) entrainment in the second case. An optimum match was obtained with deposition velocities of $v_d(H_2O_2)\approx 1.4$ cm/s and $v_d(H_2O_2)\approx 1.3$ cm/s for G04a and G07a respectively.

The sensitivity towards the entrainment rate was tested by first changing the latter to the smaller value from the CO calculations of ≈ 0.01 h^{-1}. This gives deposition velocities of <0.1 cm/s and >1.8 cm/s respectively for the two cases. A deposition velocity of <0.1 cm/s over the ocean appears very small compared to values found in the literature (see Sect. 4.4.3) and computed with the 1-D SCM. In addition, the lower entrainment rate obviously encompasses an inconsistency between the deposition velocities derived from the two cases. The deposition velocities over the ocean are expected to be similar because the BL height is the same and constant in both cases, unlike the BL over the rainforest. On the other hand, setting ER to the high value of ≈ 0.69 h^{-1} results

in unrealistically high $v_d > 10$ cm/s and $v_d > 4$ cm/s indicating that this value can only be an upper estimate for the diurnal mean entrainment rate. Both provide an indication of the magnitude of 0.12 h^{-1} for the mean entrainment rate being correct. It should be noted, however, that an average value of 1.35 cm/s for the dry deposition velocity over the ocean seems to be quite large for rather constant windspeeds of about 6 m/s. The latter result in a maximum dry deposition velocity of ≈ 0.5 cm/s in the 1-D SCM considering neutral conditions and the dependency of the windspeed on the ocean surface roughness.

4.4.2   Dry deposition velocity over the rainforest

From the Lagrangian model an estimate of the dry deposition velocity over the rainforest has been deduced, again by matching interpolated measurements at 55.86° W and model results after 24 h transport time. H_2O_2 was the only (measured) species freely calculated in the model. The median mixing ratio in the BL of the pure oceanic bin was taken as a starting value, and entrainment was included with the parameter ER set to the same value as in Sect. 4.4.1. Additionally, mean hydrogen peroxide mixing ratios for the FT of all longitudinal bins were calculated and accordingly interpolated so that a longitude dependent difference of the H_2O_2 mixing ratio between the BL and the FT was available for the longitude range examined. The dry deposition velocity was set to 1.35 cm/s over the ocean, the mean value derived in Sect. 4.4.1. Sensitivity runs with different Cl concentrations up to $30 \cdot 10^4$ cm^{-3} over the ocean revealed no significant dependence of hydrogen peroxide on halogen chemistry. Obviously, the reaction of H_2O_2 with Cl radicals is irrelevant as a sink.

An unchanged and constant value of 1.35 cm/s over the rainforest leads to an almost perfect agreement of model and measurements after 24 h transport time, while a value of 0.5 cm/s produces an overestimation of $\approx 14\%$, and a value of 2.0 cm/s an underestimation of $\approx 8\%$. The latter is probably not significant considering the accuracy of $\approx 15\%$ at 300 pmol/mol of the hydrogen peroxide measurements. The relatively strong diurnal cycle of H_2O_2 in the measurements and the Lagrangian model results, reflecting the

quite short overall lifetime of this compound in the examined environment, constitutes a further uncertainty in the estimate (see Figs. 10 and 11).

4.4.3   Comparison with results from other studies

The present study suggests a best estimate for the 24 h mean of the dry deposition velocity of hydrogen peroxide of 1.35 cm/s over the ocean as well as over the rainforest. With the values for the BL height of $\approx$400 m and $\approx$ 100–1000 m (ocean and rainforest) deposition rates of $3.25 \cdot 10^{-5}$ s^{-1} and $1.35 \cdot 10^{-5}$ up to $1.35 \cdot 10^{-4}$ s^{-1} are inferred.
  Walcek (1987) theoretically calculated a value of 1 cm/s for the H_2O_2 dry deposition velocity over the northeast United States which is roughly in agreement with our result for the rainforest and with the mean 1-D SCM result over land. Baer and Nester (1992) assessed an average $v_d(H_2O_2)$=1.5 cm/s for the region of the Upper Rhine Valley (Germany) in March 1985 with a regional mesoscale diffusion model, again relatively close to our estimate. Gao et al. (1993) used a coupled Diffusion-Chemistry-Model to calculate an H_2O_2 deposition velocity of 2.5 cm/s above a forest, about twice our value. Heikes et al. (1996) deduce a deposition of $(4 \pm 4) \cdot 10^{10}$ cm^{-2} s^{-1} for H_2O_2 and $(1.1 \pm 0.5) \cdot 10^{10}$ cm^{-2} s^{-1} for CH_3OOH from measurement data over the South Atlantic. At the given typical wind speed of 7 m/s at 10 m a.s.l. this corresponds to deposition velocities of 0.88 and 0.5 cm/s respectively, the first value for H_2O_2 being smaller than our estimate. Also the derived deposition rate of $1.4 \cdot 10^{-5}$ s^{-1} for H_2O_2 ($6 \cdot 10^{-6}$ s^{-1} for CH_3OOH) at a marine BL height of 700 m is rather smaller than our value. From gradient measurements (modified Bowen method) Hall and Claiborn (1997) compute diurnal maxima of v_d=5 cm/s for H_2O_2 and 1.6 cm/s for organic peroxide as well as nocturnal values of 1 cm/s and 0.5 cm/s respectively over a coniferous forest in Canada. Their results showed that the surface resistance is negligible in the case of H_2O_2 and that the dry deposition of all peroxides is limited by turbulence. Sillman et al. (1998) derive a dry deposition velocity of $\approx$5 cm/s for H_2O_2 from correlations of O_3, NO_z and peroxides during the Middle Tennessee Ozone Study (model and measurements), again signif-

icantly higher than the value found in the present study. Junkermann and Stockwell (1999) estimate hydrogen peroxide and methyl hydroperoxide dry deposition rates of $1 \cdot 10^{-5}$ s^{-1} and $0.8 \cdot 10^{-5}$ s^{-1} above the tropical South Atlantic in October and November 1994. The value for H_2O_2 is about a third of the value deduced in the present study.

5 However, at that time the uncertainties in chemical rate constants were still too high to make an exact estimate according to the authors. Additionally, the entrainment rate in our study could be overestimated over the ocean, as it was calculated as a 24 h mean value mainly over land and as the entrainment over the ocean may be smaller due to the generally higher stability towards vertical exchange.

10 Valverde-Canossa et al. (2006) deduced an average daylight $v_d(H_2O_2)$ of (5 ± 2) cm/s over a Norway spruce forest in the Fichtelgebirge (Germany) with the relaxed eddy-accumulation technique (REA), representing an upper limit for the diurnal average due to the generally less intense nighttime turbulence over land. Like the study by Hall and Claiborn (1997), their results indicate that daytime H_2O_2 dry deposition is lim-

15 ited by turbulence, similar to the dry deposition of HNO_3, and that it can be accurately represented by the combination of an aerodynamic and a quasi-laminar boundary resistance alone. In line with these observations, $v_d(H_2O_2)$ was found to be significantly underestimated by the 1-D SCM used in the present study when applying a relatively high surface uptake resistance (Ganzeveld et al., 2006b), whereas the disagreement

20 diminished when implementing a very small uptake resistance. Table 5 gives a synopsis of all studies including our results. To summarise, our estimate for the dry deposition velocity over the ocean is rather higher than previous estimates as well as the 1-D SCM result, probably representing an upper limit because of the relatively high entrainment rate assumed in our calculations. Our estimate of the dry deposition velocity over the

25 rainforest, on the other hand, is within and rather at the lower end of the range of results for land surfaces from other studies (1–5 cm/s). It furthermore agrees well with the result of the 1-D SCM. It should be noted that the present study focusses on dry deposition since precipitation was absent along the studied air mass trajectories.

4.5 Organic peroxides

4.5.1 Modelling the longitudinal gradient

As shown in Sect. 4.1, the measured organic peroxides show a distinct longitudinal gradient during GABRIEL, similar to CO and formaldehyde. To investigate if this gradient can be explained by photochemical degradation of organic precursors escaping the forest canopy, the Lagrangian model was used to calculate the change of the mixing ratio along the 57 trajectories. As in the hydrogen peroxide model run a constant entrainment rate of $0.12\,h^{-1}$ from the FT was assumed, and the longitude dependent FT mixing ratios were determined. A lower dry deposition rate than for H_2O_2 was used, namely $0.68 \cdot v_d(H_2O_2)=0.92$ cm/s over the ocean (average ratio $v_d(H_2O_2)/v_d(ROOH)$ from Junkermann and Stockwell (1999) and Heikes et al. (1996) above the South Atlantic) and $0.41 \cdot v_d(H_2O_2)=0.55$ cm/s over the land (diurnal average ratio $v_d(H_2O_2)/v_d(ROOH)$ following Hall and Claiborn, 1997). The modelled organic peroxides CH_3OOH, ISOOH and MVKOOH were initialised to their measured medians in the ocean bin, i.e. the total measured organic peroxide for CH_3OOH and zero for both other peroxides. Since the organic peroxides at 1–3 km a.s.l. do not exhibit an increase from east to west we have assumed that they consist only of CH_3OOH.

Figures 12 to 16 show the results for the reference run. The model predicted diurnal cycle for CH_3OOH is similar to the expected one. Maximum and minimum values are in relatively good agreement and the amplitude of the cycle also matches quite well, particularly when taking into account that the night values of the expected cycle have been deduced with the simplified approach of linear interpolation of the daylight values.

For ISOOH and MVKOOH the agreement is not so good. Especially on the second day ISOOH is obviously strongly overestimated (model peak 500–600 pmol/mol, expected $\approx$275 pmol/mol). Also for MVKOOH a clear overestimation emerges with the measured isoprene and MVK data as input, although this data has already been adjusted downward as mentioned above (model maximum 530–800 pmol/mol compared to the expected $\approx$275 pmol/mol).

The reference run results in a mean longitudinal gradient of the total organic peroxide during the 24 h transport time of 1.81 pmol/mol km^{-1} compared to 0.94 pmol/mol km^{-1} expected from the measurements.

We conclude that with the assumptions made the modelled total organic peroxide mixing ratio has to be considered inconsistent with the measurements, indicating a significantly lower mixing ratio. The formation of ISOOH from isoprene alone points at the possibility of an overestimation of isoprene by the measurements or that the chemistry is not fully understood. One alternative in explaining the discrepancy might be an effective heterogeneous loss resulting in a lifetime similar to the lifetime of the organic peroxides due to gas phase chemistry alone.

4.5.2 Sensitivity study

Sensitivity studies were carried out with a) an increased entrainment rate of 0.689 h^{-1}, b) increased deposition velocities

$$v_d(\text{ISOOH}) = v_d(\text{MVKOOH}) \overset{!}{=} v_d(\text{H}_2\text{O}_2) \tag{7}$$

and c) halved isoprene and MVK mixing ratios.

The first sensitivity run a) still produces too high mixing ratios for ISOOH and MVKOOH (diurnal cycle maxima of 350–500 pmol/mol for ISOOH and 250–350 pmol/mol for MVKOOH), obviously due to the short chemical lifetime of these compounds in the model. Furthermore, the CH$_3$OOH simulated and expected diurnal cycle do not match as well anymore, and the low morning minimum is overestimated because of a positive nighttime entrainment.

The second run b) results again in far too high concentrations, whereby the modelled diurnal cycle of CH$_3$OOH fits even better to the expected one during daylight than in the reference run. Even a further increase of the deposition velocity for ISOOH and MVKOOH to a value of 5 cm/s, much higher than the value derived for H$_2$O$_2$, still produces much too high values (maxima on the second day of 450–600 pmol/mol and 425–550 pmol/mol respectively).

EGU

With the third run c) we obtain a much better agreement of modelled and expected ISOOH and MVKOOH, while there is still a tendency to overestimate the relatively longer-lived MVKOOH.

The sensitivity tests corroborate the possibility that either isoprene and MVK are overestimated by the measurements, the isoprene chemistry is not completely understood or the organic peroxides are subject to efficient heterogenous loss. The latter may affect either the radical precursor species RO_x, as described in de Reus et al. (2005), or the peroxides themselves. Too high isoprene and MVK would fit to the overestimation of HCHO in the Lagrange as well as the steady state model over land, while a higher dry deposition alone cannot alleviate the discrepancy over the sea. Regarding the representation of isoprene chemistry in the used chemical mechanism some authors have reported that there can be a strong dependency of the product yields of isoprene oxidation on the complexity of the applied condensed mechanism (Paulson and Seinfeld, 1992; Barket et al., 2004; Fan and Zhang, 2004). Pöschl et al. (2000) come to the conclusion that a box model with the condensed Mainz Isoprene Mechanism (MIM) included also in MECCA v0.1p produces rather lower organic peroxide mixing ratios under tropical low NO_x conditions compared to the extended Master Chemical Mechanism (MCM). Nevertheless, the differences between MIM and MCM results were mostly found to be less than 10–20% for key chemical species including CH_3OOH throughout the test scenarios. The deviations in that study could be assigned mainly to a different representation of organic nitrate chemistry. von Kuhlmann et al. (2004) confirm that this is in principle also valid for the 3-D CTM MATCH-MPIC.

Thornton et al. (2002), on the other hand, found that a too large product of the branching ratio and the rate constant for organic peroxide formation via $RO_2 + HO_2$ was responsible for discrepancies found between model-predicted and measured ozone production rates. Later Hasson et al. (2004) suggested the formation of other products than peroxides including OH from the reaction of $CH_3C(O)O_2 + HO_2$. Their suggestion has recently been confirmed in laboratory kinetics measurements, and the respective reaction of the peroxy radical of MVK with HO_2 is expected to follow a similar reaction

path (J. Crowley and co-workers, private communication). To estimate possible effects on the organic peroxides, the reaction

$$MVKO_2+HO_2 \rightarrow MVKOOH+O_2 \tag{R7}$$
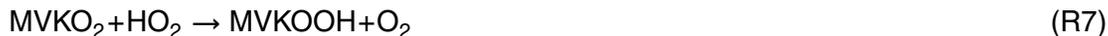
in the MECCA chemical mechanism has been substituted by an analogon of the reaction of $MVKO_2$ with NO

$$MVKO_2+HO_2 \rightarrow 0.5\,MVKOOH+0.5\,OH$$
$$+0.125\,CH_3C(O)O_2+0.125\,HOCH_2C(O)CH_3$$
$$+0.375\,HCHO+0.125\,CO+0.375\,HO_2$$
$$+0.25\,CH_3C(O)CHO \tag{R8}$$
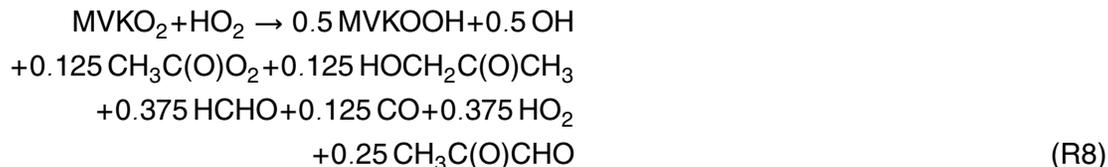
with the reaction rate unchanged compared to Reaction R7. The implementation leads to a reduced difference of only 179 pptv between modelled and expected total organic peroxide after 24 h transport time, compared to 371 pptv with the original mechanism. This is mainly due to a significantly lower predicted MVKOOH mixing ratio.

Taking into account all available information discussed up to this point, either a modified chemical mechanism like the one proposed above, leading to a reduction of the organic peroxide production, or heterogeneous loss seem to be the most likely explanations for the lower than predicted organic peroxide mixing ratio, particularly since the short chemical lifetime of ISOOH and MVKOOH makes these compounds weakly sensitive or almost insensitive towards changes in ER and v_d.

4.6 Net BL ozone production

The net ozone production (NOP) in the BL above the ocean and the rainforest was calculated using the steady state model. The last day of a series of 7 days total runtime was chosen to represent steady state. After that period all important species were found to be in dynamic equilibrium. Cl chemistry was included and the time resolution of the output decreased to 5 min. Figure 17 displays the results for the 6 cases G04a to G07c.

For case G04a ozone destruction prevails during the entire day with a maximum rate of ≈ 0.5 nmol/mol h^{-1}. The integrated NOP for daylight hours is –4 nmol/mol. Case G04b shows O_3 destruction between sunrise and about 08:00 LT with a maximum rate of ≈ 0.325 nmol/mol h^{-1} followed by a significant NOP rise up to 1.25 nmol/mol h^{-1} (coincident with the NO peak at $\approx$10:25 LT). Subsequently the NOP decreases again to negative values from $\approx$11:25 LT onward. The integrated O_3 production is –0.29 nmol/mol. Case G04c exhibits a similar evolution as case G04b but shifted to higher values in the region of destruction, leading to a positive integrated NOP of +3.33 nmol/mol. In contrast to case G04a case G07a is characterised by ozone production rather than ozone destruction, due to the higher NO mixing ratios in the second case (integrated NOP +4.4 nmol/mol). While the median NO mixing ratio is 5 pmol/mol at the time of the measurement (14:45–15:00 LT) for case G04a, it is 19 pmol/mol (11:30–11:45 LT) for case G07a. This results in a difference of almost 20 pmol/mol at a fixed local time in the expected diurnal cycles for both flight segments. Finally, cases G07b and G07c (integrated NOP +4.69 and +2.03 nmol/mol) resemble again case G04b.

Thus it appears that minor ozone production as well as destruction are in principle possible in the BL over the Atlantic Ocean northeast of the Guyanas, depending on the particular NO mixing ratio on a certain day. Nevertheless the assumption in case G07a of an NO mixing ratio rising from 19 pmol/mol in the morning up to almost 30 pmol/mol around noon appears rather improbable. The measurements on the respective flight leg may potentially have been influenced by upwind emissions from ships. Altogether, a tendency for ozone destruction is expected in the unpolluted air.

The second result is that in the BL above the rainforest a tendency for ozone production is observable. In all land cases except G04b the integrated NOP is positive during daytime depending on the actual height of the diurnal cycle NO peak. In turn, the measured median NO mixing ratios are smaller during flight G04 than during flight G07. The NOP in all 6 cases follows closely the NO diurnal cycle. The calculated average chemical tendency of +2.44 nmol/mol d^{-1} over land for the two flights is even smaller than the observed increase of the BL median mixing ratio of ozone from the

Chemistry, transport and dry deposition of trace gases during GABRIEL

A. Stickler et al.

EGU

morning to the evening for all flights of roughly 5 nmol/mol, although it does not yet compensate for the effect of dry deposition of ozone. Also the longitudinal gradient with an increase from east to west (Fig. 3) fits nicely to the positive NOP. This is again in line with the finding that mixing-in of FT air into the BL, especially during the day-time, is an important process in defining the mixing ratio of medium- up to longer-lived compounds in the BL over the tropical rainforest, since the ozone mixing ratios in the layer between 1–3 km altitude (20–50 nmol/mol) are significantly higher than in the BL with local maxima at 2–3.5 km, similar to CO. The finding of net ozone production over the quite remote rainforest region of the Guyanas in the long dry season (August to November) is in contrast to the ozone destruction of 5%/h during daytime reported for the same region from measurements at two ground based stations in Suriname in the short dry season (February and March) during LBA-CLAIRE98 (Quesada et al., 2001). The overall destruction of ozone was explained with a combination of very low photochemical production and strong dry deposition.

As can be anticipated from the diurnal cycle of the NOP following closely the NO mixing ratio, a strong positive correlation is found between these two variables in the steady state box model (Fig. 18). It can also be seen that a higher radiation intensity results in a steeper slope of the correlation.

5 Conclusions

Significant longitudinal gradients with an increase from east to west were found for CO, O_3, HCHO and organic peroxide mixing ratios in the BL over the tropical Atlantic Ocean and the Guyanas during GABRIEL. The gradient of CO derived from the longitude de-pendent medians is about twice as high (54 pmol/mol km^{-1}) as during LBA-CLAIRE98. By analysing single flights we find CO gradients of 16–48 pmol/mol km^{-1}, and a gradi-ent of 17.5 pmol/mol km^{-1} has been obtained from a "quasi Lagrangian" case identified in the measurement data.

A Lagrangian box model for CO clearly underestimates this gradient (5.6 pmol/mol

km^{-1}). Provided the chemistry is represented correctly in the model this implies that there must be other sources of CO in the BL. A sensitivity study suggests that the model-measurement discrepancies cannot be explained by measurement errors alone. Three processes potentially influencing the carbon monoxide mixing ratio in the BL

5 were examined: biomass burning, emissions from soil and vegetation and entrainment from the FT. According to this study biomass burning in parts of Africa and/or eastern Brazil can explain the relatively high CO found during several flights at an altitude of 2–3 km a.s.l.. No indication was found for an important influence of local biomass burning. An upper estimate of the effect of soil and plant emissions showed that these, together

10 with photochemistry, can probably still not account for the full range of observed CO gradients. Nonetheless they can significantly contribute to the CO budget in the BL and even regionally outbalance the photochemical production. An upper limit estimate for the 24 h mean entrainment rate from the FT into the BL of $ER=0.15$ h^{-1} was derived from the horizontal gradient and the BL-FT difference of the mixing ratio of CO, leading

15 to a better agreement of model and measurements.

A steady state and a Lagrangian model for HCHO were used to cross-check the results obtained from the CO analysis. The dry deposition velocity was adopted from a 1-D SCM. The model runs in both cases showed a significant overestimation of the HCHO mixing ratio. A deficiency of the chemical mechanism or an underestimation

20 of precursors is precluded, at least for all compounds being oxidised via formaldehyde to form CO. An underestimation of the entrainment and perhaps of the dry deposition velocity were found to be the most likely reasons for the differences. From the two models lower limits for the maximum daytime entrainment rate of $max(ER_{\mathrm{daytime}})>0.549$ h^{-1} and $max(ER_{\mathrm{daytime}})>0.689$ h^{-1} have been calculated, implying an efficient mixing-in of

25 FT air into the BL during daylight. The estimate would become smaller with a more efficient dry deposition though.

An H$_2$O$_2$ dry deposition velocity of 1.35 cm/s over the ocean as well as the rainforest has been calculated with the box model assuming an entrainment rate $ER=0.12$ h^{-1}. Sensitivity tests with a changed entrainment rate further support the correctness of the

estimated 24 h average entrainment rate. A comparison of our results with results of other studies reveals that the dry deposition velocity over the ocean is rather larger than previously derived, representing an upper limit because of the applied relatively high entrainment rate. Over the rainforest our value is within the range of previous estimates (1–5 cm/s) and rather at the lower end. Additionally, it agrees well with the explicitly computed 1-D SCM values.

The Lagrangian box model has furthermore been applied to simulate the organic peroxide longitudinal gradient assuming they only consist of methyl hydroperoxide and peroxides from isoprene and MVK oxidation. This simulation shows a significant over-estimation of the organic peroxide production in the model. Further analysis leads to the conclusion that either heterogeneous loss of organic peroxides and/or their radical precursors on aerosol particles or a modified reaction of HO_2 with $MVKO_2$ in the chemical mechanism can probably explain the discrepancies.

Finally, the net ozone production (NOP) has been calculated with the steady state model. The results indicate that over the tropical Atlantic Ocean ozone destruction rather than production prevails although there can obviously be situations with production, possibly influenced by upwind Atlantic ship emissions. Over the rainforest on average ozone production with a rate of approximately 2.4 nmol/mol d^{-1} was found. The positive NOP over the rainforest in the long dry season contrasts with results for the short dry season in the same region during LBA-CLAIRE98.

Appendix A: Abbreviations and Acronyms

ABLE	**A**tmospheric **B**oundary **L**ayer **E**xperiment
BL	**b**oundary **l**ayer
CCF	**c**loud **c**orrection **f**actor
CMDL	**C**limate **M**onitoring and **D**iagnostics **L**aboratory
CTM	**C**hemistry **T**ransport **M**odel
DL	**d**etection **l**imit
ECHAM	**EC**MWF inspired, in **Ham**burg enhanced climate model
ESRL	**E**arth **S**ystem **R**esearch **L**aboratory
FABLE	**F**ast **A**ir**b**orne **L**icor **E**xperiment
FT	**f**ree **t**roposphere
GABRIEL	**G**uyanas **A**tmosphere-**B**iosphere exchange and **R**adicals **I**ntensive **E**xperiment with the **L**earjet
GC-FID	**G**as **C**hromatography-**F**lame **I**onisation **D**etection
GFD	**G**esellschaft für **F**lugziel**d**arstellung
GTE	**G**lobal **T**ropospheric **E**xperiment
HORUS	**H**ydr**o**xyl **R**adical Measurement **U**nit based on Fluorescence **S**pectroscopy
ISON	nitrates from isoprene oxidation
ISOOH	peroxides from isoprene oxidation
LBA-CLAIRE	**L**arge-Scale **B**iosphere-**A**tmosphere Exchange Experiment-**C**ooperative **L**BA **Ai**rborne **R**egional **E**xperiment
LIF	**L**aser **I**nduced **F**luorescence
LT	**l**ocal **t**ime
MATCH-MPIC	**M**odel of **A**tmospheric **T**ransport and **Ch**emistry - **M**ax **P**lanck **I**nstitute for **C**hemistry version

EGU

MCM	**M**aster **C**hemical **M**echanism
MECCA	**M**odule **E**fficiently **C**alculating the **C**hemistry of the **A**tmosphere
MEK	**m**ethyl **e**thyl **k**etone
MEKOOH	peroxides from MEK oxidation
MIM	**M**ainz **I**soprene **M**echanism
MODIS	**Mod**erate Resolution **I**maging **S**pectroradiometer
MPAN	peroxyacryloyl nitrate
MVK	**m**ethyl **v**inyl **k**etone
MVKOOH	peroxides from MVK oxidation
NACA	**n**itrooxy **a**cet**a**ldehyde
NIWA	**N**ational **I**nstitute of **W**ater and **A**tmospheric Research (New Zealand)
NMOC	**n**on-**m**ethane **o**rganic **c**ompound
NOP	**n**et **o**zone **p**roduction
ONIT	organic nitrate from higher alkyl nitrates and C_3H_6 + NO_3
PAN	**p**eroxy**a**cetyl **n**itrate
PTFE	**p**oly **t**etra **f**luoro **e**thylen
PTR-MS	**P**roton **T**ransfer **R**eaction-**M**ass **S**pectrometer
SCM	**S**ingle **C**olumn **M**odel
TDLAS	**T**unable **D**iode **L**aser **A**bsorption **S**pectrometer
TRISTAR	**Tr**acer **I**n-**s**itu **T**DLAS for **A**tmospheric **R**esearch
TUV	**T**ropospheric **U**ltraviolet-**V**isible Model
VOC	**v**olatile **o**rganic **c**ompound
UTOPIHAN	**U**pper **T**ropospheric **O**zone: **P**rocesses **I**nvolving **HO**x **a**nd **NO**x

EGU

Chemistry, transport and dry deposition of trace gases during GABRIEL

A. Stickler et al.

Title Page

Abstract	Introduction
Conclusions	References
Tables	Figures

◄ | ►|

◄ | ►

Back | Close

Full Screen / Esc

Printer-friendly Version

Interactive Discussion

EGU

References

Baer, M. and Nester, K.: Parameterization of trace gas dry deposition velocities for a regional mesoscale diffusion model, Ann. Geophysicae, 10, 912–923, 1992. 4814, 4837

Barket, D. J., Grossenbacher, J. W., Hurst, J. M., Shepson, P. B., Olszyna, K., Thornberry, T., Carroll, M. A., Roberts, J., Stroud, C., Bottenheim, J., and Biesenthal, T.: A study of the NO_x dependence of isoprene oxidation, J. Geophys. Res., 109, D11310, 2004. 4818

Brenninkmeijer, C. A. M., Koeppel, C., Röckmann, T., Scharffe, D. S., Bräunlich, M., and Gros, V.: Absolute measurement of the abundance of atmospheric carbon monoxide, J. Geophys. Res., 106, 10 003–10 010, 2001. 4785

Carvalho, L. R. F., Vasconcellos, P. C., Mantovani, W., Pool, C. S., and Pisani, S. O.: Measurements of biogenic hydrocarbons and carbonyl compounds emitted by forest trees from temperate warm Atlantic rainforest, Brazil, J. Environ. Monit., 7, 493–499, 2005. 4783

Chang, C.-T., Liu, T.-H., and Jeng, F.-T.: Atmospheric concentrations of the Cl atom, ClO radical, and HO radical in the coastal marine boundary layer, Environ. Res., 94, 67–74, 2004. 4798

Chatfield, R. B., Vastano, J. A., Li, L., Sachse, G. W., and Connors, V. S.: The Great African plume from biomass burning: Generalizations from a three-dimensional study of TRACE A carbon monoxide, J. Geophys. Res., 103, 28 059–28 077, 1998. 4805

Conrad, R. and Seiler, W.: Influence of temperature, moisture, and organic carbon on the flux of H_2 and CO between soil and atmosphere: Field studies in subtropical regions, J. Geophys. Res., 90, 5699–5709, 1985. 4805

de Reus, M., Fischer, H., Sander, R., Gros, V., Kormann, R., Salisbury, G., van Dingenen, R., Williams, J., Zöllner, M., and Lelieveld, J.: Observations and model calculations of trace gas scavenging in a dense Saharan dust plume during MINATROC, Atmos. Chem. Phys., 5, 1787–1803, 2005, http://www.atmos-chem-phys.net/5/1787/2005/. 4809, 4818

Faloona, I.: Observations of HO_x and its relationship with NO_x in the upper troposphere during SONEX, J. Geophys. Res., 105, 3771–3783, 2000.

Fan, J. and Zhang, R.: Atmospheric oxidation mechanism of isoprene, Environ. Chem., 1, 140–149, 2004. 4818

Fehsenfeld, F., Calvert, J., Fall, R., Goldan, P., Guenther, A. B., Hewitt, C. N., Lamb, B., Liu, S., Trainer, M., Westberg, H., and Zimmerman, P.: Emissions of volatile organic compounds from vegetation and the implications for atmospheric chemistry, Global Biogeochem. Cycles,

Title Page

Abstract | Introduction

Conclusions | References

Tables | Figures

◄◄ | ►►

◄ | ►

Back | Close

Full Screen / Esc

Printer-friendly Version

Interactive Discussion

EGU

6, 389–430, 1992. 4783

Finlayson-Pitts, B. J. and Pitts, J. N., eds.: Chemistry of the Upper and Lower Atmosphere, Academic Press, London (UK), 2000. 4783, 4792, 4798, 4801

Ganzeveld, L., Klemm, O., Rappenglück, B., and Valverde-Canossa, J.: Evaluation of meteorological parameters over a coniferous forest in a single-column chemistry-climate model, Atmos. Environ., 40, S21–S27, doi:10.1016/j.atmosenv.2006.01.061, 2006a. 4783, 4796

Ganzeveld, L., Valverde-Canossa, J., Moortgat, G. K., and Steinbrecher, R.: Evaluation of peroxide exchanges over a coniferous forest in a single-column chemistry-climate model, Atmos. Environ., 40, S68–S80, doi:10.1016/j.atmosenv.2006.01.062, 2006b. 4783, 4796, 4815

Ganzeveld, L. N., Lelieveld, J., Dentener, F. J., Krol, M. C., and Roelofs, G.-J.: Atmosphere-biosphere trace gas exchanges simulated with a single-column model, J. Geophys. Res., 107, doi:10.1029/2001JD000684, 2002. 4796

Gao, W., Wesely, M. L., and Doskey, P. V.: Numerical modeling of the turbulent diffusion and chemistry of NO_x, O_3, isoprene, and other reactive trace gases in and above a forest canopy, J. Geophys. Res., 98, 18 339–18 353, 1993. 4814, 4837

Greenberg, J. P. and Zimmerman, P. R.: Nonmethane hydrocarbons in remote tropical, continental, and marine atmospheres, J. Geophys. Res., 89, 4767–4778, 1984. 4790

Hall, B. D. and Claiborn, C. S.: Measurements of the dry deposition of peroxides to a Canadian boreal forest, J. Geophys. Res., 102, 29 343–29 353, 1997. 4814, 4815, 4816, 4837

Hasson, A. S., Tyndall, G. S., and Orlando, J. J.: A product yield study of the reaction of HO_2 radicals with ethyl peroxy ($C_2H_5O_2$), acetyl peroxy ($CH_3C(O)O_2$), and acetonyl peroxy ($CH_3C(O)CH_2O_2$) radicals, J. Phys. Chem. A, 108, 5979–5989, 2004. 4818

Heikes, B., Lee, M., Jacob, D., Talbot, R., Bradshaw, J., Singh, H., Blake, D., Anderson, B., Fuelberg, H., and Thompson, A. M.: Ozone, hydroperoxides, oxides of nitrogen, and hydrocarbon budgets in the marine boundary layer over the South Atlantic, J. Geophys. Res., 101, 24 221–24 234, 1996. 4814, 4816, 4837

Helas, G., Bingemer, H., and Andreae, M. O.: Organic-acids over equatorial Africa — Results from DECAFE-88, J. Geophys. Res., 97, 6187–6193, 1992. 4801

Holton, J. R., ed.: An Introduction to Dynamic Meteorology, vol. 48 of *International Geophysics Series*, Academic Press, London (UK), 1992. 4784

Jacob, D. J. and Wofsy, S. C.: Photochemistry of biogenic emissions over the Amazon forest, J. Geophys. Res., 93, 1477–1486, 1988. 4802

Chemistry, transport and dry deposition of trace gases during GABRIEL

A. Stickler et al.

Title Page

Abstract	Introduction
Conclusions	References
Tables	Figures

◄◄   ►►

◄   ►

Back   Close

Full Screen / Esc

Printer-friendly Version

Interactive Discussion

EGU

Jacob, D. J. and Wofsy, S. C.: Budgets of reactive nitrogen, hydrocarbons, and ozone over the Amazon-forest during the wet season, J. Geophys. Res., 95, 16 737–16 754, 1990. 4801, 4802

Junkermann, W. and Stockwell, W. R.: On the budget of photooxidants in the marine boundary layer of the tropical South Atlantic, J. Geophys. Res., 104, 8039–8046, 1999. 4815, 4816, 4837

Kesselmeier, J. and Staudt, M.: Biogenic volatile organic compounds (VOC): An overview on emission, physiology and ecology, J. Atmos. Chem., 33, 23–88, 1999. 4783

Kirchhoff, V. W. J. H. and Marinho, E. V. A.: Surface carbon monoxide measurements in Amazonia, J. Geophys. Res., 95, 16 933–16 943, 1990. 4805

Krinke, S. M. W.: Experimentelle Bestimmung der Depositionsgeschwindigkeit von Formaldehyd und Ozon über einem Laubwaldbestand, PhD thesis, University Stuttgart, Faculty of Chemistry, 1999. 4812

Lazrus, A. L., Kok, G. L., Gitlin, S. N., and Lind, J. A.: Automated fluorometric method for hydrogen peroxide in atmospheric precipitation, Anal. Chem., 57, 917–922, 1985. 4786

Lazrus, A. L., Kok, G. L., Lind, J. A., Gitlin, S. N., Heikes, B. G., and Shetter, R. E.: Automated fluorometric method for hydrogen peroxide in air, Anal. Chem., 58, 594–597, 1986. 4786

Loveland, T. R., Reed, B. C., Brown, J. F., Ohlen, D. O., Zhu, Z., Yang, L., and Merchant, J. W.: Development of a global land cover characteristics database and IGBP DISCover from 1 km AVHRR data, Int. J. Remote Sensing, 21, 1303–1330, 2000. 4783, 4806

Lowe, D. C., Allan, W., Manning, M. R., Bromley, T., Brailsford, G., Ferretti, D., Gomez, A., Knobben, R., Martin, R., Mei, Z., Moss, R., Koshy, K., and Maata, M.: Shipboard determinations of the distribution of ^{13}C in atmospheric methane in the Pacific, J. Geophys. Res., 104, 26 125–26 135, 1999. 4798

Madronich, S. and Flocke, S.: The role of solar radiation in atmospheric chemistry, in: Handbook of Environmental Chemistry, edited by: Boule, P., pp. 1–26, Springer, Heidelberg, 1998. 4789

McKeen, S. A., Gierczak, T., Burkholder, J. R., Wennberg, P. O., Hanisco, T. F., Keim, E. R., Gao, R.-S., Liu, S. C., Ravishankara, A. R., and Fahey, D. W.: The photochemistry of acetone in the upper troposphere: A source of odd-hydrogen radicals, Geophys. Res. Lett., 24, 3177–3180, 1997.

Padhy, P. K. and Varshney, C. K.: Isoprene emission from tropical tree species, Environmental Pollution, 135, 101–109, 2005. 4783

Chemistry, transport and dry deposition of trace gases during GABRIEL

A. Stickler et al.

Title Page

Abstract	Introduction
Conclusions	References
Tables	Figures

|◄ | ►|

◄ | ►

Back | Close

Full Screen / Esc

Printer-friendly Version

Interactive Discussion

EGU

Paulson, S. E. and Seinfeld, J. H.: Development and evaluation of a photooxidation mechanism for isoprene, J. Geophys. Res., 97, 20 703–20 715, 1992. 4818

Platt, U., Allan, W., and Lowe, D.: Hemispheric average Cl atom concentration from ^{13}C/^{12}C ratios in atmospheric methane, Atmos. Chem. Phys., 4, 2393–2399, 2004, http://www.atmos-chem-phys.net/4/2393/2004/. 4798

Pöschl, U., von Kuhlmann, R., Poisson, N., and Crutzen, P. J.: Development and intercomparison of condensed isoprene oxidation mechanisms for global atmospheric modeling, J. Atmos. Chem., 37, 29–52, 2000. 4818

Quesada, J., Grossmann, D., Fernández, E., Romero, J., Sanhueza, E., Moortgat, G., and Crutzen, P. J.: Ground based gas phase measurements in Surinam during the LBA-CLAIRE 98 experiment, J. Atmos. Chem., 39, 15–36, 2001. 4821

Roeckner, E., Arpe, K., Bengtsson, L., Christoph, M., Claussen, M., Dümenil, L., Esch, M., Giorgetta, M., Schlese, U., and Schulzweida, U.: The atmospheric general circulation model ECHAM-4: Model description and simulation of present-day climate, Tech. rep., Max-Planck-Institut für Meteorologie, Hamburg(Germany), 1996. 4796

Roeckner, E., Bengtsson, L., Feichter, J., Lelieveld, J., and Rodhe, H.: Transient climate change simulations with a coupled atmosphere-ocean GCM including the tropospheric sulfur cycle, J. Climate, 12, 3004–3032, 1999. 4796

Sander, R., Kerkweg, A., Jöckel, P., and Lelieveld, J.: Technical Note: The new comprehensive atmospheric chemistry module MECCA, Atmos. Chem. Phys., 5, 445–450, 2005, http://www.atmos-chem-phys.net/5/445/2005/. 4789

Sanhueza, E., Donoso, L., Scharffe, D., and Crutzen, P. J.: Carbon monoxide fluxes from natural, managed, or cultivated savannah grassland, J. Geophys. Res., 99, 16 421–16 427, 1994. 4805

Scharffe, D., Hao, W. M., Donoso, L., Crutzen, P. J., and Sanhueza, E.: Soil fluxes and atmospheric concentration of CO and CH$_4$ in the northern part of the Guayana Shield, Venezuela, J. Geophys. Res., 95, 22 475–22 480, 1990. 4806

Schönwiese, C.-D., ed.: Praktische Statistik für Meteorologen und Geowissenschaftler, Gebrüder Bornträger, Berlin (Germany), 1992. 4809

Sillman, S., He, D. Y., Pippin, M. R., Daum, P. H., Imre, D. G., Kleinman, L. I., Lee, J. H., and Weinstein-Lloyd, J.: Model correlations for ozone, reactive nitrogen, and peroxides fro Nashville in comparison with measurements: Implications for O$_3$-NO$_x$-hydrocarbon chemistry, J. Geophys. Res., 103, 22 629–22 644, 1998. 4814, 4837

Title Page

Abstract | Introduction

Conclusions | References

Tables | Figures

|◄ | ►|

◄ | ►

Back | Close

Full Screen / Esc

Printer-friendly Version

Interactive Discussion

EGU

Singh, H. B., Gregory, G. L., Anderson, B., Browell, E., Sachse, G. W., Davis, D. D., Crawford, J., Bradshaw, J. D., Talbot, R., Blake, D. R., Thornton, D., Newell, R., and Merrill, J.: Low ozone in the marine boundary layer of the tropical Pacific Ocean: Photochemical loss, chlorine atoms, and entrainment, J. Geophys. Res., 101, 1907–1917, 1996. 4798

Stevens, P. S.: HO_2/OH and RO_2/HO_2 rates during the Tropospheric OH Photochemistry Experiment: Measurement and theory, J. Geophys. Res., 102, 6379–6391, 1997.

Stickler, A.: HCHO, H_2O_2 und CH_3OOH in der Troposphäre, PhD thesis, Johannes Gutenberg University Mainz, Faculty of Physics, 2006. 4786, 4789

Stickler, A., Fischer, H., Williams, J., de Reus, M., Sander, R., Lawrence, M. G., Crowley, J. N., and Lelieveld, J.: Influence of summertime deep convection on formaldehyde in the middle and upper troposphere over Europe, J. Geophys. Res., 111, D14308, doi:10.1029/2005JD007001, 2006. 4783, 4786, 4789, 4790, 4791, 4792, 4793, 4794, 4795, 4802, 4803

Tao, Z. and Jain, A. K.: Modeling of global biogenic emissions for key indirect greenhouse gases and their response to atmospheric CO_2 increases and changes in land cover and climate, J. Geophys. Res., 110, D21309, doi:10.1029/2005JD005874, 2005. 4805

Tarr, M. A., Miller, W. L., and Zepp, R. G.: Direct carbon monoxide photoproduction from plant matter, J. Geophys. Res., 100, 11 403–11 413, 1995. 4806

Thornton, J. A., Wooldridge, P. J., Cohen, R. C., Martinez, M., Harder, H., Brune, W. H., Williams, E. J., Roberts, J. M., Fehsenfeld, F. C., Hall, S. R., Shetter, R. E., Wert, B. P., and Fried, A.: Ozone production rates as a function of NO_x abundances and HO_x production rates in the Nashville urban plume, J. Geophys. Res., 107, doi:10.1029/2001JD000932, 2002. 4818

Valverde-Canossa, J., Ganzeveld, L., Rappenglück, B., Steinbrecher, R., Klemm, O., Schuster, G., and Moortgat, G. K.: First measurements of H_2O_2 and organic peroxides surface fluxes by the relaxed eddy-accumulation technique, Atmos. Environ., 40, S55–S67, doi:10.1016/j.atmosenv.2006.03.038, 2006. 4815, 4837

von Glasow, R., Sander, R., Bott, A., and Crutzen, P. J.: Modeling halogen chemistry in the marine boundary layer 1. Cloud-free MBL, J. Geophys. Res., 107, doi:10.1029/2001JD000942, 2002. 4798

von Kuhlmann, R., Lawrence, M. G., Pöschl, U., and Crutzen, P. J.: Sensitivities in global scale modeling of isoprene, Atmos. Chem. Phys., 4, 1–17, 2004, http://www.atmos-chem-phys.net/4/1/2004/. 4818

Walcek, C. J.: A theoretical estimate of O_3 and H_2O_2 dry deposition over the northeast United-

Title Page

Abstract | Introduction

Conclusions | References

Tables | Figures

◄ | ►

◄ | ►

Back | Close

Full Screen / Esc

Printer-friendly Version

Interactive Discussion

EGU

States, Atmos. Environ., 21, 2649–2659, 1987. 4814, 4837

Williams, J., Fischer, H., Hoor, P., Pöschl, U., Crutzen, P. J., Andreae, M. O., and Lelieveld, J.: The influence of the tropical rainforest on atmospheric CO and CO_2 as measured by aircraft over Surinam, South America, Chemosph.–Global Change Science, 3, 157–170, 2001a. 4798, 4800

Williams, J., Pöschl, U., Crutzen, P. J., Hansel, A., Holzinger, R., Warneke, C., Lindinger, W., and Lelieveld, J.: An atmospheric chemistry interpretation of mass scans obtained from a Proton Transfer Mass Spectrometer flown over the tropical rainforest of Surinam, J. Atmos. Chem., 38, 133–166, 2001b. 4802

Wingenter, O. W., Kubo, M. K., Blake, N. J., Smith, T. W., Blake, D. R., and Rowland, F. S.: Hydrocarbon and halocarbon measurements as photochemical and dynamical indicators of atmospheric hydroxyl, atomic chlorine, and vertical mixing obtained during Lagrangian flights, J. Geophys. Res., 101, 4331–4340, 1996. 4798

Zimmerman, P. R., Greenberg, J. P., and Westberg, C. E.: Measurements of atmospheric hydrocarbons and biogenic emission fluxes in the Amazon boundary layer, J. Geophys. Res., 93, 1407–1416, 1988. 4790

Chemistry, transport and dry deposition of trace gases during GABRIEL

A. Stickler et al.

Table 1. Synopsis of measured species during the GABRIEL campaign

Species	Measurement technique	DL [nmol/mol]	Precision	Accuracy	Systematic error [%]
CO	TDLAS	0.2		2.5%	
HCHO	TDLAS	0.25	25%	26.9%	
H_2O_2	derivatisation + fluorimetry	0.029	9.7%	14.8%	< +25–30
ROOH	derivatisation + fluorimetry	<0.029	<9.7%	25.9%	
OH	LIF	0.00002	0.000035 pmol/mol	40% (56%)	
HO_2	LIF	0.00007	0.0005 pmol/mol	60%	
NO	chemiluminescence	0.005		12%	
O_3	chemiluminescence	2		2%	
$J(NO_2)$	filter radiometer		1%	10%	
CH_3OH	PTR-MS	0.269	39%	5–10% (excl. prec.)	
CH_3CN	PTR-MS	0.068	20%	5–10% (excl. prec.)	
$CH_3C(O)CH_3$	PTR-MS	0.094	17%	5–10% (excl. prec.)	
isoprene	PTR-MS	0.099	7%	5–10% (excl. prec.)	
MVK	PTR-MS	0.093	12%	5–10% (excl. prec.)	
H_2O	LI-COR	200000		5%	
CO_2	LI-COR			0.3 μmol/mol	

Title Page

Abstract | Introduction

Conclusions | References

Tables | Figures

|◄ | ►|

◄ | ►

Back | Close

Full Screen / Esc

Printer-friendly Version

Interactive Discussion

EGU

Table 2. Median measured CO longitudinal gradients during flights G03, G04 and G07; the median at 55.86° W was derived by a linear interpolation of the values at 55° W and 56° W

Flight	G03	G04	G07
Median CO 51.5° W [nmol/mol]	102.0	95.1	82.2
Median CO 55.86° W [nmol/mol]	109.7	110.7	105.6
$\Delta CO/\Delta x$ [pmol/mol km^{-1}]	16	32	48

Table 3. Sensitivities of CO to different chemical species; [1]during nighttime only, [2]diurnal average, [3]constant value, [4]nitrooxy acetaldehyde, [5]organic nitrate from the isoprene oxidation, [6]methyl ethyl ketone, [7]organic nitrate from higher alkyl nitrates and $C_3H_6 + NO_3$, [8]i-propyl nitrate

Parameter	Variation Parameter [nmol/mol]	Variation CO [nmol/mol]	Sensitivity [(nmol/mol)/(nmol/mol)]
NO_3	$+0.01$[1]	-0.4517	-45.17
NO	$+0.0024$[2]	$+0.0666$	27.75
HCHO	$+0.3805$[2]	$+2.6285$	6.908
MVK	$+0.258$[2]	$+0.9933$	3.85
MVKOOH	$+0.865$[2]	$+2.7046$	3.124
NACA[4]	$+0.5$[3]	$+1.1302$	2.2604
$CH_3C(O)CH_2OOH$	$+0.865$[2]	$+0.7978$	0.922
ISON[5]	$+0.5$[3]	$+0.3849$	0.7698
C_3H_6	$+0.336$[3]	$+0.2219$	0.6604
CH_3CHO	$+4.845$[3]	$+3.1208$	0.644
$C_3H_6(OH)OOH$	$+0.865$[2]	$+0.4797$	0.555
$CH_3C(O)CH_2OH$	-0.550[3]	-0.2923	0.531
isoprene	$+0.478$[2]	$+0.2328$	0.487
C_4H_9OOH	$+0.865$[2]	$+0.3704$	0.428
C_2H_5OOH	$+0.865$[2]	$+0.3459$	0.400
MEK[6]	$+1.798$[3]	$+0.5379$	0.299
MEKOOH	$+0.865$[2]	$+0.2433$	0.281
ONIT[7]	$+0.05$[3]	$+0.01$	0.14
C_2H_4	$+2.6$[3]	$+0.2658$	0.1022
CH_3OOH	$+0.865$[2]	$+0.0775$	0.0896
$CH_3C(O)OH$	$+5$[3]	$+0.0739$	0.01478
HNO_3	$+0.25$[3]	$\|<0.0001$	$\|<0.0004$
$C_3H_7(O)NO_2$[8]	$+0.05$[3]	$\|<0.0001$	$\|<0.0002$
ISOOH	$+0.865$[2]	0	0
C_3H_7OOH	$+0.865$[2]	$\|<0.002$	$\|<0.002$

Table 4. Comparison of the average measured HCHO mixing ratios during the six cases defined in Sect. 3.3 with the steady state mixing ratios predicted by the box model for the reference run and cases with: OH decreased by 25%; increased HO_2 (25%); NO decreased by 5 pmol/mol; dry deposition velocity increased by 50% (equivalent to a BL height decreased by 33.3%); OH, NO and Cl decreased (the latter by 75%) and dry deposition velocity increased respectively; the model runs were done with yet uncorrected radiation data, however, the reference run including J values with a correction factor of 1.1 gives results only slightly smaller (<7%); the results of case G07c have to be taken with caution since methanol, isoprene and acetone mixing ratios had to be estimated due to lacking PTR-MS data

Case	G04a	G04b	G04c	G07a	G07b	G07c
Mean measured HCHO (1σ empirical SD[1]) [pmol/mol]	328 (259)	983 (262)	1041 (220)	367 (134)	496 (166)	632 (140)
HCHO RR[2] [pmol/mol]	510	1492	1667	701	734	691
OH ↓ [pmol/mol]	431	1181	1323	580	593	548
HO_2 ↑ [pmol/mol]	461	1301	1438	650	653	613
NO ↓ [pmol/mol]	377	1366	1513	641	641	608
v_d ↑ (BL height ↓) [pmol/mol]	495	1434	1602	638	646	651
OH ↓, NO ↓, Cl ↓, $v_d = v_d(HNO_3)$ [pmol/mol]	312	975	1079	522	335	386

[1]SD: estimated error (standard deviation) of the mean, calculated as $\sigma_{n-1}(HCHO)/\sqrt{n}$ with the number of measurement points n on the respective flight segment, [2]RR: reference run

EGU

Table 5. H_2O_2 dry deposition velocities $v_d(H_2O_2)$ and respective BL deposition rates found over land and over sea surfaces in different studies. $v_{d,l}(H_2O_2)$: dry deposition velocity over land, $v_{d,s}(H_2O_2)$: dry deposition velocity over the sea. For detailed information and discussion of the different results see text.

Reference	$v_{d,l}(H_2O_2)$ [cm/s]	$v_{d,s}(H_2O_2)$ [cm/s]	Deposition rate [s^{-1}]	Region
Walcek (1987)	1			NE United States
Baer and Nester (1992)	1.5			Upper Rhine Valley (Germany)
Gao et al. (1993)	2.5			above forest
Heikes et al. (1996)		0.88	$1.4 \cdot 10^{-5}$	South Atlantic
Hall and Claiborn (1997)	1-5			coniferous forest in Canada
Sillman et al. (1998)	≈ 5			Tennessee
Junkermann and Stockwell (1999)			$1 \cdot 10^{-5}$	tropical South Atlantic
Valverde-Canossa et al. (2006)	(5 ± 2)			Fichtelgebirge (Germany)
This study	1.35	1.35	$1.35 \cdot 10^{-5...4}$ (land)	tropical rainforest
			$3.25 \cdot 10^{-5}$ (sea)	tropical Atlantic
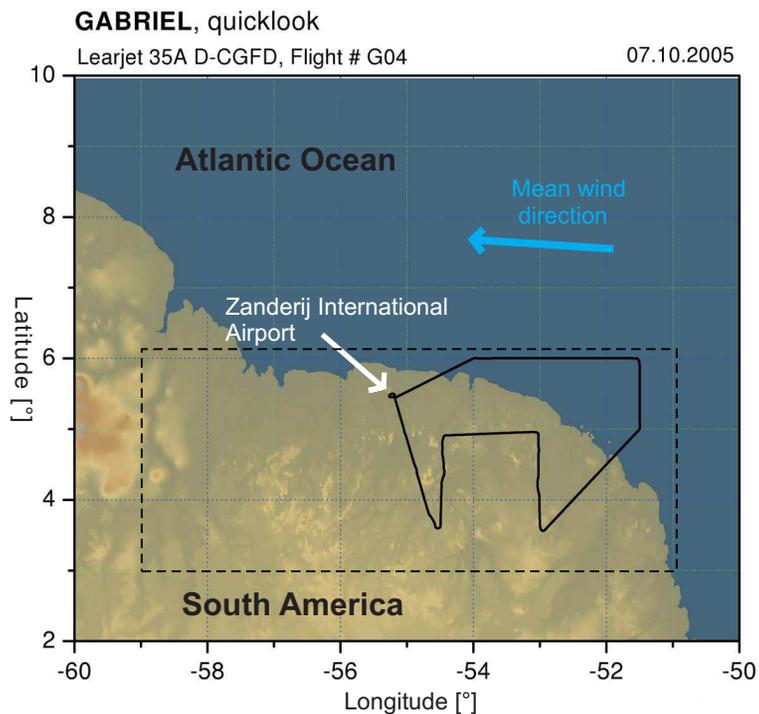
Fig. 1. Operations area (black dashed rectangle) of the Learjet 35A during the GABRIEL campaign. The flight track of flight G04 is indicated by a black line. The north-south flight legs are (from east to west) the segments G04a, G04b and G04c. The map shows part of the Guyana Highlands (in the west and south), the coastal plains of Guyana, Suriname and French Guyana. The track of flight G07 is almost identical to that of G04.
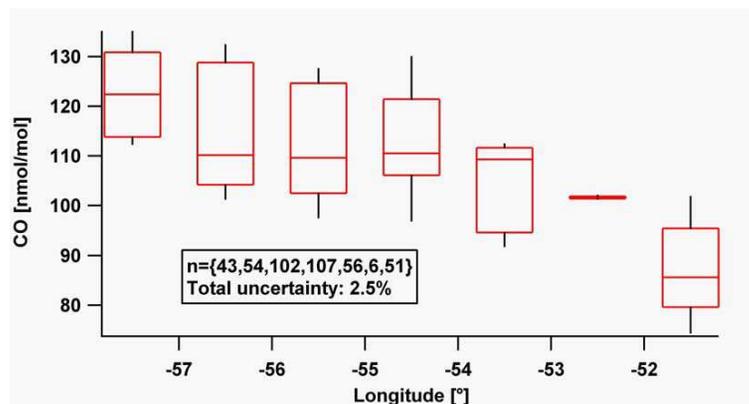
Fig. 2. Longitudinal profile of the CO median mixing ratio in the altitude range 0–1 km a.s.l.; red bar denotes the median; the lower and upper boundary of the red box mark the 25% and 75% percentiles, the bottom and top whisker the 10% and 90% percentiles.
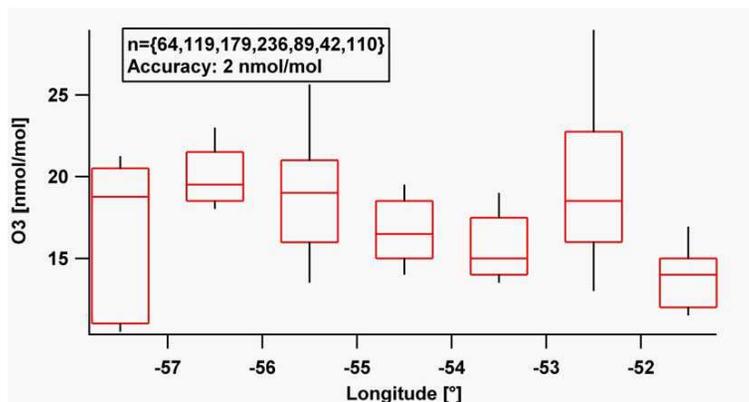
Fig. 3. Longitudinal profile of the O$_3$ median mixing ratio in the altitude range 0–1 km a.s.l.; as Fig. 2.
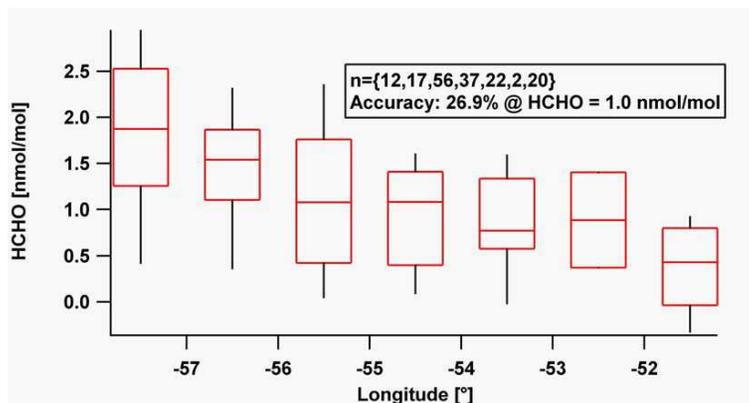
Fig. 4. Longitudinal profile of the HCHO median mixing ratio in the altitude range 0–1 km a.s.l.; as Fig. 2.
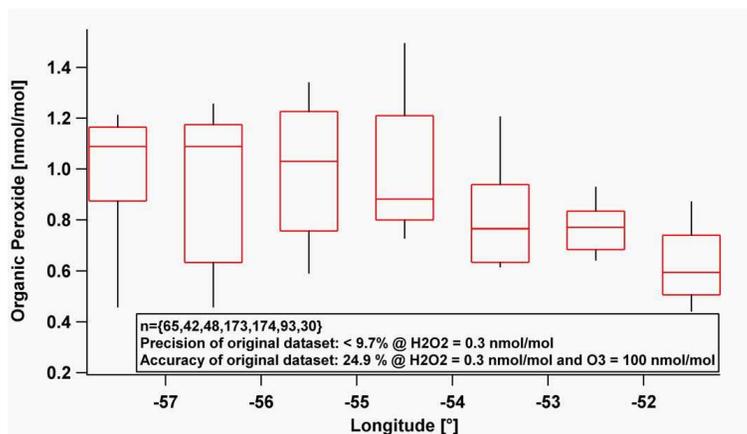
Fig. 5. Longitudinal profile of the total organic peroxide median mixing ratio in the altitude range 0–1 km a.s.l.; as Fig. 2.

EGU
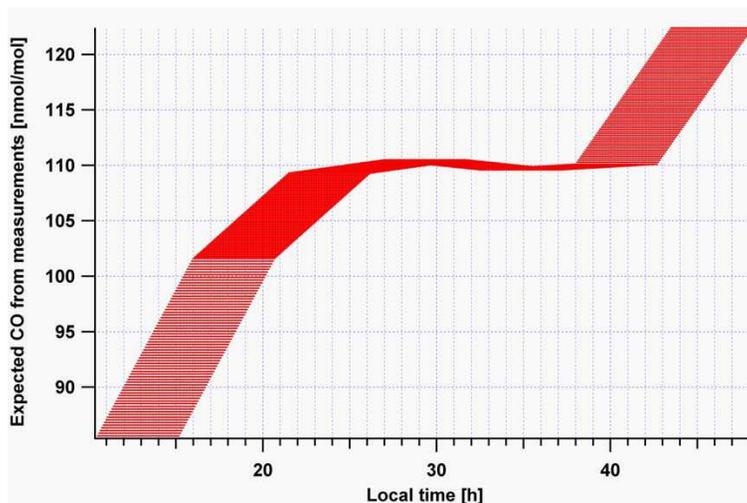
Fig. 6. Expected CO mixing ratios along the 57 different trajectories prescribed by the varying *k* values; the variation of the mixing ratio as a function of local time arises solely from the measured longitudinal gradient, superimposed by the effect of the different starting times of the trajectories.

Fig. 7. CO mixing ratios calculated along the 57 different trajectories with the box model (Lagrangian mode, reference run).

Fig. 8. Expected HCHO mixing ratios along the 57 different trajectories prescribed by the varying *k* values; the variation of the mixing ratio as a function of local time arises from the measured longitudinal gradient, the effect of the different starting times of the trajectories and the superimposed diurnal cycle.
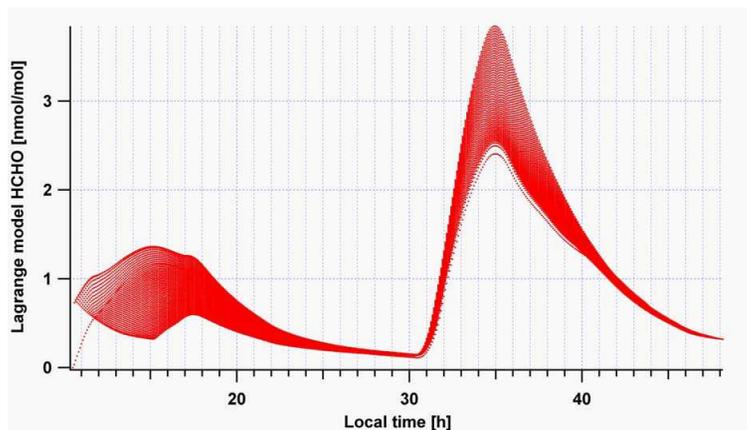
Fig. 9. HCHO mixing ratios calculated along the 57 different trajectories with the box model (Lagrangian mode, reference run).

Fig. 10. Expected H_2O_2 mixing ratios along the 57 different trajectories prescribed by the varying k values. The variation of the mixing ratio as a function of local time arises from the measured longitudinal gradient, the effect of the different starting times of the trajectories and the superimposed diurnal cycle.
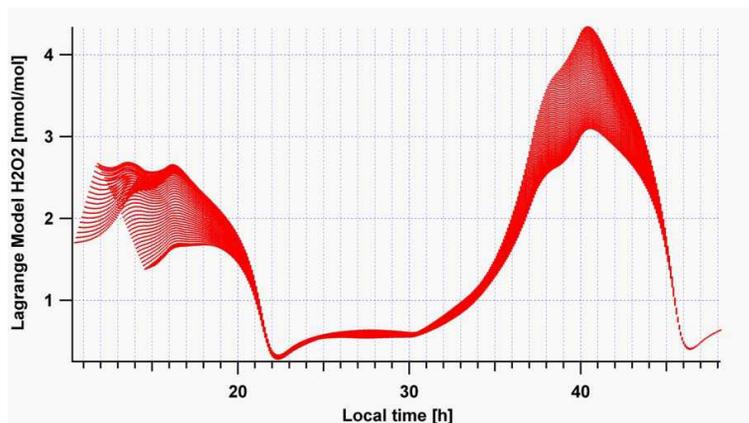
Fig. 11. H_2O_2 mixing ratios calculated along the 57 different trajectories with the box model (Lagrangian mode, reference run).

Fig. 12. Expected CH$_3$OOH mixing ratios along the 57 different trajectories prescribed by the varying k values. The variation of the mixing ratio as a function of local time arises from the measured longitudinal gradient, the effect of the different starting times of the trajectories and the superimposed diurnal cycle.

EGU

Fig. 13. CH$_3$OOH mixing ratios calculated along the 57 different trajectories with the box model (Lagrangian mode, reference run).

Fig. 14. Expected ISOOH/MVKOOH mixing ratios along the 57 different trajectories prescribed by the varying k values. the variation of the mixing ratio as a function of local time arises from the measured longitudinal gradient, the effect of the different starting times of the trajectories and the superimposed diurnal cycle.
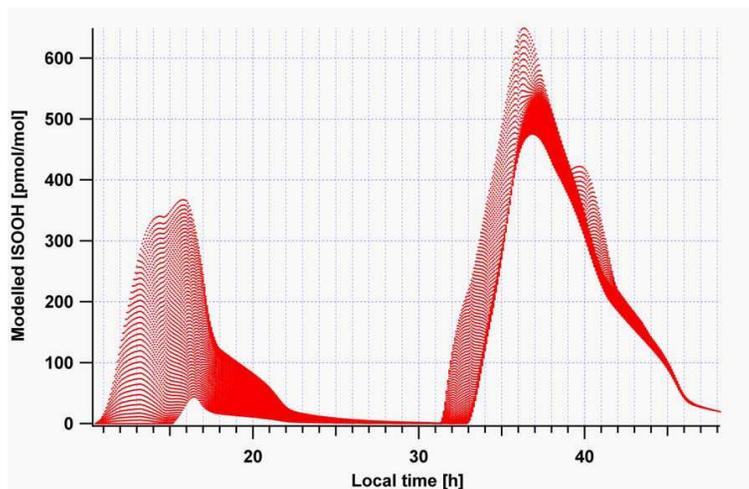
Fig. 15. ISOOH mixing ratios calculated along the 57 different trajectories with the box model (Lagrangian mode, reference run).

Title Page

Abstract | Introduction

Conclusions | References

Tables | Figures

◄ | ►

◄ | ►

Back | Close

Full Screen / Esc

Printer-friendly Version

Interactive Discussion

Fig. 16. MVKOOH mixing ratios calculated along the 57 different trajectories with the box model (Lagrangian mode, reference run).

EGU

ACPD

7, 4781–4855, 2007

Chemistry, transport
and dry deposition of
trace gases during
GABRIEL

A. Stickler et al.

Title Page

Abstract | Introduction

Conclusions | References

Tables | Figures

|◄ | ►|

◄ | ►

Back | Close

Full Screen / Esc

Printer-friendly Version

Interactive Discussion

EGU
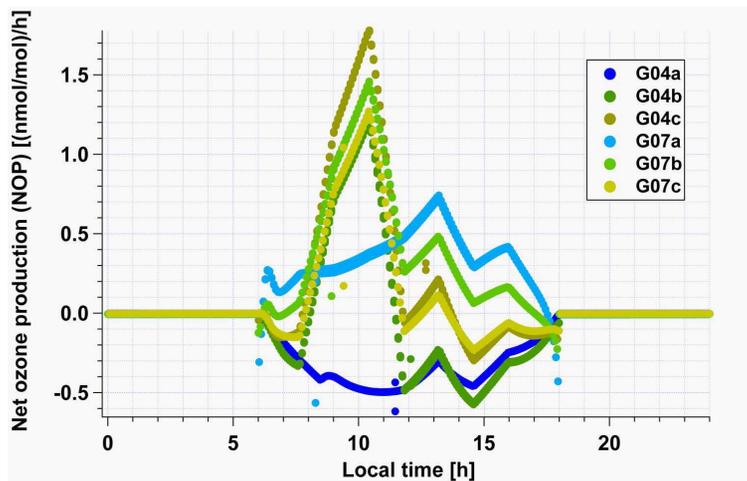
Fig. 17. Net ozone production calculated with the steady state box model for the 6 cases defined in Sect. 3.3.
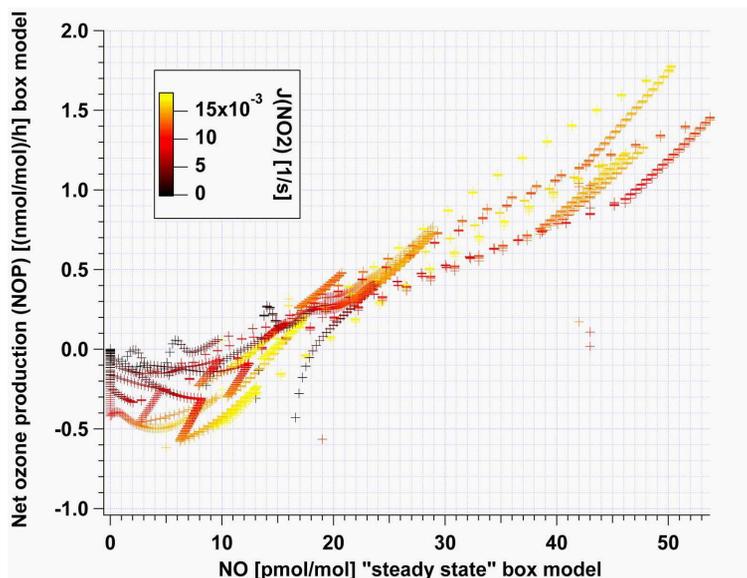
Fig. 18. Correlation between the net ozone production (NOP) and the NO mixing ratio in the "steady state" box model, colourcoded depending on the value of $J(NO_2)$.